Continental Shelf Research 50–51 (2012) 80–99

Contents lists available at SciVerse ScienceDirect

Continental Shelf Research

journal homepage: www.elsevier.com/locate/csr

Research papers

Evaluation of the numerical wave model (SWAN) for wave simulation in the Black Sea

Adem Akpınar [a,*], Gerbrant Ph. van Vledder [b,c], Murat İhsan Kömürcü [d], Mehmet Özger [e]

[a] Gümüşhane University, Civil Engineering Department, 29000 Gümüşhane, Turkey
[b] Delft University of Technology, Civil Engineering and Geosciences Department, The Netherlands
[c] BMT Argoss, Vollenhove, The Netherlands
[d] Karadeniz Technical University, Civil Engineering Department, 61080 Trabzon, Turkey
[e] İstanbul Technical University, Civil Engineering Department, 34469 İstanbul, Turkey

ARTICLE INFO

Article history:
Received 11 February 2012
Received in revised form
25 September 2012
Accepted 26 September 2012
Available online 7 October 2012

Keywords:
Wave prediction and simulation
Shallow water processes
SWAN model
JONSWAP method
Black Sea

ABSTRACT

This study summaries the implementation of the SWAN model forced by the ECMWF ERA Interim dataset reanalyzed 10 m winds over the Black Sea which will be used to study the wind-wave climate and wave energy potential in the region, and its verification. The SWAN model results were compared with directional buoy measurements at three locations along the north and south coasts of the Black Sea, parametric model results based on the JONSWAP growth relations, and the results of previous studies. The SWAN model has been applied in a third generation and non-stationary mode with spherical coordinates. The linear and exponential growth from wind input, depth-induced wave breaking, bottom friction, whitecapping, four-wave (for deep water) and triad-wave (for shallow water) nonlinear interactions have been activated in the simulations. The results of this study indicate that agreement between simulated and observed wave parameters is satisfactory and it is slightly more accurate than the results of the previous studies. However, it still has lower estimates for the maximum values of both wave parameters. These lower estimates are probably due to too low wind speeds in the applied ECMWF wind fields, which is probably caused by orographic effects, and due to the relatively course resolution in time and space of the ECMWF (ERA-Interim) wind fields for the Black Sea.

1. Introduction

The sustainable development of economic activities in the marine environment requires long-term data about environmental conditions such as wind-generated waves. Accordingly, the knowledge of the wind-wave climate is necessary in a variety of applications including design of coastal structures, sediment transport, coastal erosion and pollution transport studies. Due to the lack of measurements in many regions, wind-wave characteristics are estimated using different methods, especially numerical models (Moeini and Etemad-Shahidi, 2007).

Countries that border the Black Sea have put a lot of scientific efforts to investigate the wind and wave climate of the sea for several decades. The results of former research on the wind and wave climate of the Black Sea have been published in many handbooks and monographs (Rzheplinkskij, 1969; Sorkina, 1974; Terziev, 1991, etc.). However, presented statistical estimates are based on limited and sparse field data that increase the uncertainity of the obtained wind and wave regime (Valchev, 2008). Besides, the first international research that included scientific institutions from all countries near the Black Sea was the NATO TU-WAVE project (Özhan and Abdalla, 1998). The project was carried out for the construction of long-term and extreme wind and wave climate of the Black Sea basin. The hindcast wave modelling of the project was accomplished using Middle East Technical University 3 (METU3) (Abdalla and Özhan, 1994) and WAM (WAMDI Group, 1988; Özhan et al., 2003) models. The time span for the long-term and the analysis of extreme statistics was 8 and 20 years, respectively (Cherneva et al., 2008). The European Centre for Medium-Range Weather Forecasts (ECMWF) has also been running a version of the WAM model for the Black Sea with the purpose of forecasting. Cherneva et al. (2008) developed a WAM Cycle 4 wave model for the conditions of the Black Sea and validated the model by using field data. Despite these attempts to develop wave forecasting systems for the Black Sea, and in view of recent progress in forecasting capabilities (e.g., Cavaleri et al., 2007), we consider these systems not fully applicable for the present needs of providing accurate forecasts. Also, the previous studies include only offshore conditions. In recent years, progress

* Corresponding author. Tel.: +90 456 233 7425x1146; fax: +90 456 233 7427.
E-mail addresses: aakpinar@ktu.edu.tr, aakpinar@gumushane.edu.tr (A. Akpınar).

0278-4343/$ - see front matter
http://dx.doi.org/10.1016/j.csr.2012.09.012

in forecasting capabilities and improvements on the accuracy of hindcast wind fields enables us to implement more accurate 3rd generation (3G) models, including both offshore and nearshore conditions. In the Black Sea, there have been a few attempts to implement the SWAN model for various engineering purposes. Rusu (2009) assessed the wave energy resources by focusing on the western part of the Black Sea. Rusu (2010a) evaluated oil spills propagation in the coastal environment of the Black Sea. Rusu (2010b) modelled wave-current interactions at the mouths of the Danube Delta in the Black Sea. Rusu and Ivan (2010) studied modelling wind waves in the Romanian coastal environment.

Therefore, the aim of this study is to implement and validate a wind-wave numerical model for the Black Sea, which will be used to study the wave climate, perform extreme value analysis, and determine the wave energy potential in the region. As known, a quantitative knowledge about the wave climate at any given location is very important for modelling (for example, modelling littoral sand transport), planning the construction of offshore structures (for example, the computation of the probability of calm sea states), navigation purposes, and coastal management alike. Besides, the scientists or engineers need to better understand the wave climate and extreme value conditions at any region because they influence the long-term resilience of offshore engineering structures and coastal wave impacts. Therefore, having an accurate model is of great importance to the scientific and engineering community and this study sets and validates the model to perform the further works. The Simulating WAves Nearshore (SWAN) model (Booij et al., 1999) has been selected for application in this case given that it is successfully applied (internationally) by numerous users for the offshore and shallow waters of different seas. Further, The Turkish State Meteorological Service has shown their interest in using the SWAN model for their forecasting services. The wave model is forced by the ERA Interim dataset, which is the latest global atmospheric reanalysis produced by the ECMWF (Dee et al., 2011), reanalyzed 10 m winds. The wave model performance of our Black Sea SWAN model is assessed by considering different wave periods for each buoy station by the quantification of differences between simulated wave parameters and buoy measurements gathered at three locations along the south and north coasts of the Black Sea. The SWAN model predictions were also compared with results of the METU3 model (Abdalla et al., 1995) for only a 1-month period (unfortunately no additional data were available), the WAM Cycle 4 model (Cherneva et al., 2008) for three different measuring periods at three locations, and a parametric model based on the JONSWAP growth relations (Hasselmann et al., 1973) applied to two buoy stations.

The paper includes the backgrounds of the applied wave prediction models, description of the study area, the used data sets, and the SWAN wave model set-up. Then, the SWAN model validation and comparison against the buoy data, JONSWAP method and the previous studies results will be presented to assess quality of the generated wave data in this study. The directional dependence of wave model performance with respect to wind direction and shallow water aspects will be discussed. Finally, conclusions and recommendations will be presented.

2. Wave prediction methods

2.1. Empirical-based methods

Until now, several empirical methods such as PM (Pierson and Moskowitz, 1964), Wilson (Wilson, 1965), SMB (Bretschneider, 1970), JONSWAP (Hasselmann et al., 1973), Donelan (Donelan, 1980), SPM (US Army, 1984), Kahma and Calkoen (1992), and CEM (US Army, 2003) have been developed and proposed for the prediction or forecasting of sea states. Parametric methods are relatively good as long as they are used for open seas and steady winds, but they fail in areas with directionally dependent upwind fetch restrictions and non-homogeneous and temporal wind systems. Another disadvantage of such methods is that they only provide information on integral parameters such as the significant wave height or an average wave period, but no spectral information. Further, they usually assume that the mean wave direction is equal to the wind direction. Only full spectral methods like WAM (WAMDI Group, 1988), Wavewatch (Tolman, 1991), or SWAN (Booij et al., 1999) are able to provide such detailed information. In this study, the SWAN model is compared with the result of the JONSWAP method, which is a commonly used parametric wave prediction model.

In all empirical methods, it is assumed that the generation of wind waves is mainly a function of three parameters which are wind speed, fetch length, and wind duration. In fetch-limited conditions, wave parameters are a function of wind speed and fetch length only. On the other hand, wind duration variable is required for determining the duration-limited waves. These methods have been developed based on interrelationship among dimensionless wave parameters (Kazeminezhad et al., 2005). Therefore, in the prediction of wave parameters, the required variables can be taken as wind speed, fetch length, and wind duration (Özger and Şen, 2007).

2.1.1. Fetch length

Wind fetch length is defined as the unobstructed distance that wind can travel over water in a constant direction, which varies depending on the upwind directions. In the areas with coastal irregularities such as an inlet, gulf, and embayment, different methods were described in the literature to take into account the effect of the neighbouring coasts to determine an effective fetch length. The concept of effective fetch assumes that, waves are generated over a 45° range either side of the wind direction and energy transfer from wind to waves is proportional to the cosine of the angle between the wind and wave directions, and wave growth is proportional to the fetch length. Hence,

$$F_{effective} = \frac{\sum F_i \ \cos^2 \ \alpha_i}{\sum \cos \ \alpha_i} \tag{1}$$

where $F_{effective}$ is the effective fetch and is the length to be used in the all parametric methods for open seas. F_i and α_i are fetch lengths and angles measured at 7.5° interval, respectively (Yüksel and Çevik, 2009; Reeve et al., 2004).

2.1.2. Determinating of wind blowing duration

To determine the duration of winds, the definition of constant wind was used according to (US Army, 2003). In this way, wind duration at ith hourly data point was considered to be equal to the number of preceeding consecutive hours satisfying the following criteria:

$$|U_{\mathrm{i}} - \overline{U}| < 2.5 \quad \mathrm{m/s} \tag{2}$$

$$|D_i - \overline{D}| < 15^o \tag{3}$$

where $\overline{U}$ and $\overline{D}$ are the average of preceding consecutive and acceptable hourly wind speed and direction, respectively. U_i and D_i are the wind speed and direction at ith hourly data point (Kazeminezhad et al., 2005). Note that in case of rapidly changing wind conditions, less and less points will satisfy these requirements, thus limiting the reliability of this method.

2.1.3. JONSWAP wave prediction method

The JONSWAP method predicts parametrically the integral wave parameters. These parameters are then used to define the spectrum, using the JONSWAP shape. This spectrum is frequently used to describe waves in a growing phase. The form of the spectrum is defined in terms of the peak frequency rather than the wind speed as (Hasselmann et al., 1973):

$$E(f)=\alpha g^2(2\pi)^{-4}f^{-5}\ \exp\left[-\frac{5}{4}\left(\frac{f}{f_p}\right)^{-4}\right]\gamma^{\exp\left[-(f-f_p)^2/2\sigma^2 f_p^2\right]} \tag{4}$$

where

$$\alpha=0.076\left(g\,FU^{-2}\right)^{-0.22} \tag{5}$$

$$f_p\ =\ \frac{3.5\ g\ \left(g\ F\ U^{-2}\right)^{-0.33}}{U} \tag{6}$$

$$\sigma=\begin{Bmatrix} 0.07 & f<f_p \\ 0.09 & f\geq f_p \end{Bmatrix} \tag{7}$$

f_p and U are the frequency of spectral peak and wind speed at 10 m above mean water level. The alpha sets the level of the high frequency tail and the gamma and sigma variables represent the peak enhancement of the spectral peak of the wind sea and the narrowness of this peak, respectively. The mean value of gamma during the JONSWAP experiment was observed to be 3.3, but in practise this parameter depends on the growth stage of the waves. Significant wave height (H_s) and mean zero up-crossing wave period (T_z) are defined for the fetch-limited case as follows:

$$H_s=0.0163\,F^{1/2}\,U \tag{8}$$

$$T_z=0.439F^{3/10}U^{2/5} \tag{9}$$

and for the duration-limited case,

$$H_s=0.0146\,t^{5/7}\,U^{9/7} \tag{10}$$

$$T_z=0.419t^{3/7}U^{4/7} \tag{11}$$

where H_s, T_z, F, and t are in m, s, km, and hour. Fetch-limited formulaes are appropriate if the following equation is satisfied:

$$t>1.167\,F^{0.7}/U^{0.4} \tag{12}$$

Otherwise, equations for duration-limited case are used (Özger, 2007; Özger and Şen, 2007).

2.2. Numerical-based models

With increasing knowledge of wave processes, several sophisticated numerical wave models have been developed. Starting with first-generation models, we have now reached the stage of fully discrete third generation spectral models such as WAM (WAMDI Group, 1988), SWAN (Booij et al., 1999), WAVEWATCH III (Tolman, 1999). These wave prediction models are applied from ocean to coastal scales. The essence of a 3G model is that no restrictions are imposed on the spectral shape and that it is fully determined by the source terms. The SWAN model has widely been used all over the world from coastal engineers in many coastal wave studies, especially because of its ease of use and its unconditionally stable numerical scheme. Besides, it is a method that The Turkish State Meteorological Service has recently been interested into to be applied for their forecasting services. Therefore, this study is focused on the SWAN model to perform wave simulations in the Black Sea.

2.2.1. The SWAN model

The SWAN model is a numerical third-generation wave model that provides realistic estimates of wave parameters in open seas, coastal areas, lakes, and estuaries from given wind-, bottom, and current conditions. Holthuijsen et al. (1993), Ris et al. (1999), Booij et al. (1999), and Zijlema and Van der Westhuysen (2005) describe the theoretical and numerical background.

The SWAN model calculates the development of a sea state by means of action density $N(\sigma,\theta)$ rather than by means of variance density $E(\sigma,\theta)$, as in the presence of currents action density is conserved whereas variance density is not. Action density is equal to variance density divided by relative frequency ($N=E/\sigma$) (Booij et al., 1999). The independent variables are the relative frequency σ (as observed in a frame of reference moving with the current velocity) and the wave direction θ (the direction normal to the wave crests). In the SWAN wave model, the evolution of the wave spectrum is described by an Eulerian formulation of the balance of wave energy density. In the Eulerian energy balance approach, the balance of wave energy is considered in predefined cells in a grid. The balance of energy prescribes that within every grid cell of size $\Delta x\Delta y$, and over a time interval Δt:

$$\begin{aligned}\textit{Change of energy} &= \textit{Net import of energy}\\ &\quad + \textit{Net local generation}\end{aligned} \tag{13}$$

The application of this principle leads to the following expression, valid for every frequency-direction component in the spectrum, which is known as the energy balance equation, for deep water and in the absence of currents:

$$\frac{\partial}{\partial t}E+\frac{\partial}{\partial x}(c_xE)+\frac{\partial}{\partial y}(c_yE)=S(\sigma,\theta;x,y,t) \tag{14}$$

where c_x and c_y are x, y components of the group velocity corrected for propagation on a current with velocity and $S(\sigma,\theta;x,y,t)$ is source term which represents all effects of generation and dissipation (Booij et al., 1999; Van der Westhuysen, 2002).

If the energy balance equation is applied to shallow coastal regions and for ambient currents, it is converted to the spectral action balance equation for shallow water as follows:

$$\frac{\partial}{\partial t}N+\frac{\partial}{\partial x}(c_xN)+\frac{\partial}{\partial y}(c_yN)+\frac{\partial}{\partial \sigma}(c_\sigma N)+\frac{\partial}{\partial \theta}(c_\theta N)=\frac{S(\sigma,\theta;\,x,y,t)}{\sigma} \tag{15}$$

The first term in the left-hand side of this equation represents the rate of change of action in time and the second and third terms represent the propagation of action in geographical space (x, y). The fourth and fifth terms represent the frequency shift and refraction induced by depth and currents, respectively. The source/sink term $S(\sigma,\theta)$, on the right-hand side of the action balance equation, represents the effects of generation, dissipation, and nonlinear wave–wave interactions. It is usually given by

$$\begin{aligned}S(\sigma,\theta)=&S_{inp}(\sigma,\theta)+S_{brk}(\sigma,\theta)+S_{frc}(\sigma,\theta)+S_{wcp}(\sigma,\theta)\\ &+S_{nl3}(\sigma,\theta)+S_{nl4}(\sigma,\theta)\end{aligned} \tag{16}$$

These terms denote, respectively, generation due to wind input, dissipations due to depth-induced wave breaking, bottom friction, and whitecapping, and triad and quadruplet nonlinear wave–wave interactions (WAMDI Group, 1988; Cavaleri et al., 2007). Details of these processes can be found in the SWAN manual (SWAN team, 2012).

2.2.2. Functionality of the SWAN model

Expressions for Eqs. (15) and (16) are the core of the 3G wave prediction model SWAN taking into account the following propagation processes; propagation through geographic space, refraction due to spatial variations in bottom and current, shoaling due to spatial variations in bottom and current. In addition special features are built-in for wave reflection by opposing currents, and transmission through, blockage by or reflection against obstacles, and diffraction effects. Generally, two types of mechanisms, namely the linear growth mechanism due to Phillips (1957) and the exponential growth mechanism due to Miles (1957), can be distinguished that describe the transfer of wind energy and momentum to the wave field through the action of atmospheric pressure fluctuations. Based on these two growth mechanisms, wave growth by wind is commonly given by the sum of linear and exponential growth term of a wave component. The linear growth term is dominant initially, but the exponential growth term quickly becomes dominant if some wave energy is present. In the SWAN model, while the expression for the linear growth term is due to Cavaleri and Malanotte-Rizzoli (1981), the corresponding expressions for the exponential growth due to Komen et al. (1984), rescaled in terms of friction velocity, and Janssen (1989, 1991) can also be used (Ris et al., 1994).

The fact that SWAN offers the user to choose between various source terms (per process) reflects the state of the art of wave modelling; we do not completely know which is the best. Therefore, depending on the users preferences, trust or experience of just tuning, one set of source terms is chosen in a certain SWAN model setup. A good description of the state of the art can be found in Cavaleri et al. (2007). Presently, a new set of source terms is being developed in various research projects which may become available in third-generation models in the coming years (e.g. Ardhuin et al., 2010; Tolman et al., 2011). However, as these new methods are still under development, they are not included in the present study.

The dissipation term of wave energy is represented by the summation of three different contributions: depth-induced breaking, bottom friction, and whitecapping. The process of depth-induced wave breaking is still poorly understood and little is known about its spectral modelling. In contrast to this, the total dissipation (i.e. integrated over the spectral space) due to this type of wave breaking can be well modelled with the dissipation of a bore applied to the breaking waves in a random field. In the SWAN model, the formulation of Battjes and Janssen (1978) is used with $\alpha=1$ and $\gamma=0.73$ (SWAN team, 2012). The process of the wave energy dissipation due to bottom friction can be estimated based on the empirical JONSWAP formulation (Hasselmann et al., 1973), the drag law model of Collins (1972) or the eddy-viscosity model of Madsen et al. (1988). The whitecapping term is derived from the model of Hasselmann (1974) which considers whitecaps as randomly distributed pressure pulses, and it is applied in adapted form of Komen et al. (1984).

Resonant sets of wave components exchange energy resulting in the distribution of wave energy over the energy density spectrum. In deep water, SWAN models this energy transfer by means of four-wave (or quadruplet) interactions and in shallow water by means of three-wave (or triad) interactions. Quadruplet–wave interaction is the main contributor to the evolution of the wave spectrum in deep water (Young and Van Vledder, 1993). By quadruplet interaction energy is transferred from the peak region to both lower frequency and higher frequencies, but also a redistribution over the directions takes place. In addition, quadruplet interaction stabilizes the spectral shape. The transfer to the forward face of the spectrum is responsible for the downshifting of the peak frequency (Hasselmann et al., 1973). This process is particularly important during situations of wind-wave generation. For the computation of this term, the Discrete Interaction Approximation (DIA) derived by Hasselmann et al. (1985), is applied in SWAN. Triad-wave interaction does not play a role in deep water, but can be significant in intermediate depths and in the shoaling zone (Battjes, 1994; Van der Westhuysen, 2002). In very shallow waters, triad wave–wave interactions transfer energy from lower frequencies to higher frequencies, often resulting in higher harmonics. A parameterization of this effect, which is the Lumped Triad Approximation (LTA) of Eldeberky and Battjes (1996), is included in the SWAN model (Moeini and Etemad-shahidi, 2009).

The integration of the action balance equation has been implemented in SWAN with finite difference schemes in all five dimensions: time, geographic space (x, y) and spectral space (σ, θ). The SWAN equations are cast in an implicit scheme and solved numerically by an iterative sweep mechanism. This feature makes the SWAN model particularly robust and suited for coastal applications. Zijlema and Van der Westhuysen (2005) present a good discussion on this topic. The SWAN model has also no courant number limitation like WAM or WAVEWATCH. Therefore, it is able to efficiently cope with small spatial resolutions in coastal applications. More details are given in the SWAN user manual (SWAN team, 2012).

In the present study the SWAN model is applied in non-stationary mode as the area of interest is too large to allow stationary computations as the time scale of wave propagation through the area of interest is larger than the time scale of changes in wind forcing. As the Black Sea is a semi-enclosed basin, no wave boundary conditions need to be specified. Further, as currents are considered very weak we did not include them in our hindcasts.

3. The study area and datasets

3.1. The study area

This study focused on all of the Black Sea, which is located between 41° and 46° north latitudes and 28° and 41.5° east longitudes. It is a semi-closed sea connecting respectively to the Sea of Marmara and Aegean Sea by the Bosphorus and Dardanels straits and also to the Sea of Azov by the strait of Kerch in the form of a kidney from west to east. It has an area of 461 thousand square kilometres (not including the Sea of Marmara but including the Sea of Azov) and 8350 km of coastline, and a maximum depth of 2588 m and also its longest extent is about 1175 km in the east–west direction. The Black Sea is one of the world's largest landlocked basins (Akpınar et al., 2011). Fig. 1 illustrates the study area and locations of the Hopa, Sinop, and Gelendzhik buoys deployed at 41°25′24″N–41°23′00″E, 42°07′24″N–35°05′12″E, and 44°30′27″N–37°58′42″E, respectively. The depths of the deployed wave buoys at the Hopa and Sinop stations are 100 m while it is 85 m for the Gelendzhik station. These buoys were deployed to collect wave data within the scope of the NATO TU-WAVES Project (Özhan and Abdalla, 1998).

3.2. Wind data

The atmospheric forcing data used as principal input to the SWAN model in this study was the 6 hourly wind fields (four analyses fields per day, at 00, 06, 12, and 18 UTC) of the u and v wind components at 10 m from the ECMWF re-analyses. Re-analyses are improved model predictions blended with direct observations. ECMWF carried out three different re-analysis projects, namely ECMWF ERA 15, ERA 40, and ERA Interim. In this study, the ECMWF ERA Interim dataset was used because it is the latest version of the re-analyses and therefore it is considered to provide the most accurate data. The results of this database is a set of gridded data (spatial resolution: 0.25° in longitude, 0.25° in latitude) with a temporal resolution of 6 h. A sample wind field from ECMWF ERA Interim dataset is shown in Fig. 2. The main advantages of the re-analyses are their physical consistency and relatively high temporal coverage (from January 1, 1979, to the present). Data of this re-analysis database is 100% coverage over a 30-year recording period (6 hourly recording intervals).

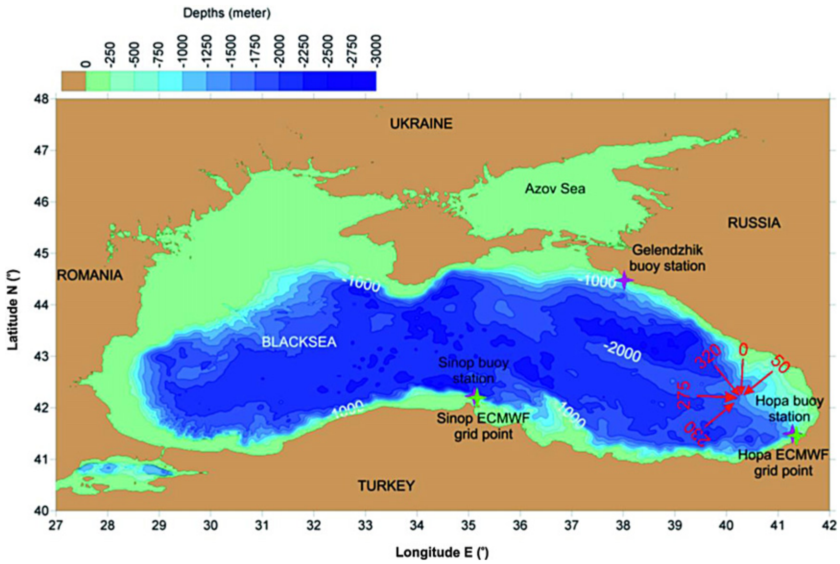

Fig. 1. The study area, bathymetry of the Black Sea (isobaths are given in meters), and the locations of buoys (in pink colour) and wind recording stations (in green colour). (For interpretation of the references to color in this figure legend, the reader is referred to the web version of this article.)

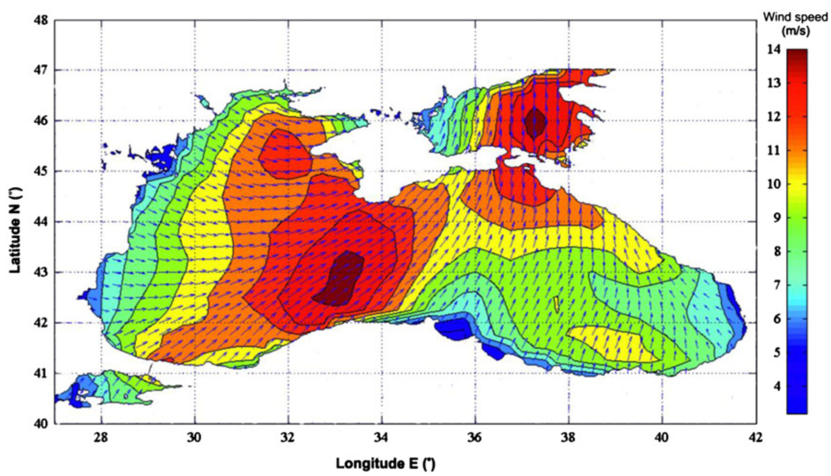

Fig. 2. A sample wind field from the ECMWF ERA Interim for at 10 m on 1 January 1995, at 00.00 h. Arrows indicate the wind direction.

Comprehensive documentation of the ECMWF re-analyses projects and the datasets can be found at http://www.ecmwf.int. Discussions about product quality of this wind re-analysis databases against others can be found in Bidlot et al. (2002), Caires et al. (2004), Signell et al. (2005). Ponce de Leon et al. (2012), and Dee et al. (2011). As a result, the ECMWF systems are considered to be the most accurate wind field available.

For the implementation of the JONSWAP method, which will be used to compare against the SWAN simulations, the time series of the wind speed and direction of the closest ECMWF grid point to the Hopa and Sinop buoy stations were used. The JONSWAP hindcasts were performed for all months of 1996 at the Hopa location and for the first 6 months of 1996 for the Sinop location as stated in Section 2.1. Figs. 3 and 4 show the temporal variations of the wind speed and direction, which were used as input data to the JONSWAP models, at the Hopa and Sinop buoy locations for the chosen time periods. The temporal ECMWF wind field data were also used as the driving force of the SWAN model. Some statistical parameters of the recorded wind data in the ECMWF ERA Interim dataset at Hopa and Sinop stations for 1996 are given in Table 1. As can be seen from the figures, there are prominent differences in trends of temporal changes of wind speed and direction. Wind speed at Hopa ECMWF grid point varies from 1 to 4 m/s, and it takes values between 2 and 6 m/s at Sinop ECMWF grid point. The maximum wind speeds are 7.2 m/s for Hopa grid point and 8.6 m/s for Sinop grid point. The average wind speeds at Hopa and Sinop grid points were recorded as 2.3 and 3.7 m/s, respectively. Hence, it can be seen that the area around Sinop grid point is exposed to more severe winds than Hopa grid point. However, these winds are still weak because wind speeds above 20 m/s seldomly occur. The dominant wind directions at these buoy locations are from southerly directions.

3.3. Wave data

In this study wave records of three directional buoy stations deployed at Hopa, Sinop, and Gelendzhik were used to verify the developed SWAN wind-wave model. The first one is the 12-month wave dataset recorded in 1996 year for the Hopa buoy station. The second and third ones are the 6-month datasets for

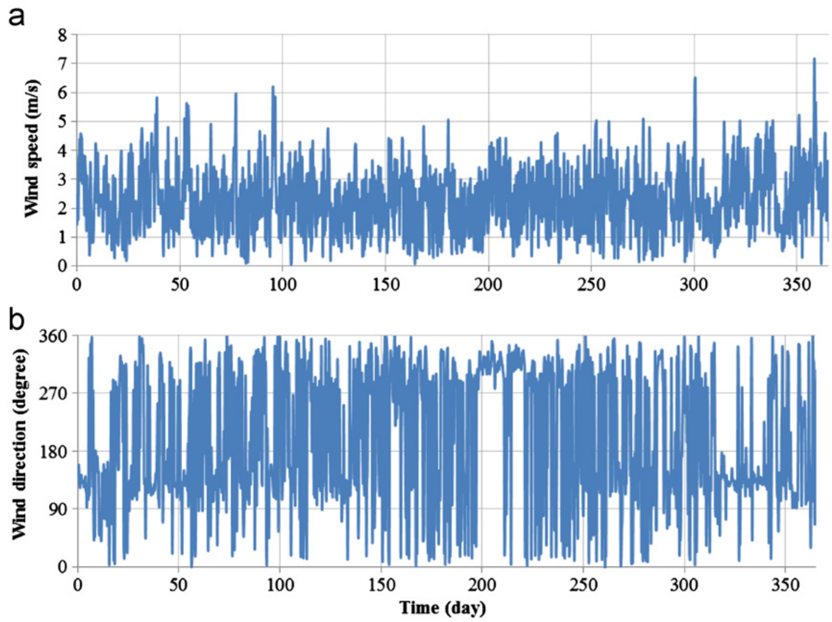

Fig. 3. Temporal variation of (a) wind speed and (b) direction for all months of 1996 (from January 1 to December 31) obtained from ERA Interim hindcast dataset of the ECMWF at the Hopa station.

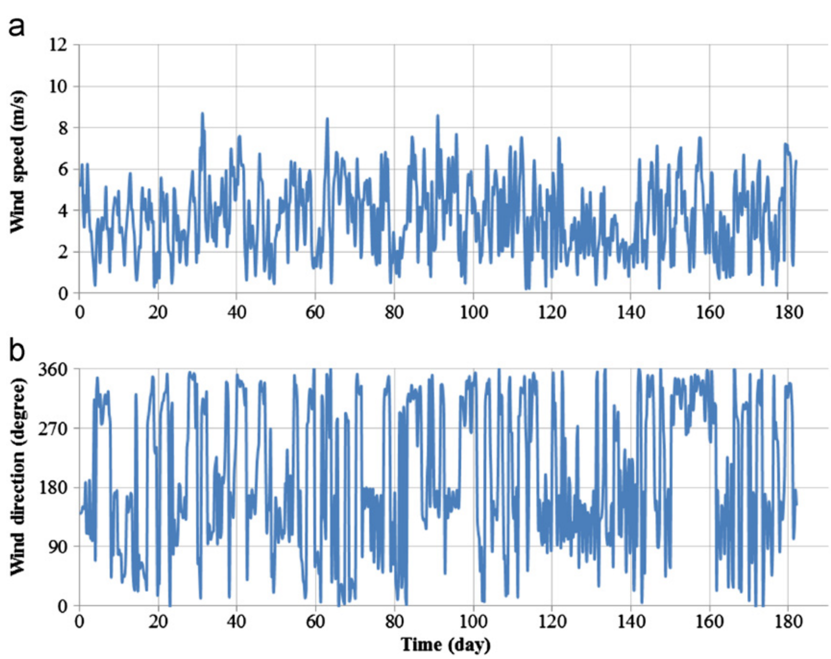

Fig. 4. Temporal variation of (a) wind speed and (b) direction for time period between January 1, 1996 and June 30, 1996 obtained from ERA Interim hindcast dataset of the ECMWF at the Sinop station.

Table 1
Statistics of recorded wind data in the ECMWF ERA Interim dataset at Hopa and Sinop stations during the considering time periods for each station.

Wind parameter	Statistical measures	Hopa station	Sinop station
Wind speed (m/s)	Minimum	0.1	0.2
	Maximum	7.2	8.6
	Average	2.3	3.7
	Standard deviation	1.2	1.8
Wind direction (°)	Minimum	0	0
	Maximum	360	360
	Average	198	199
	Standard deviation	103	108

Table 2
Locations of wave measurement stations and periods of measurements considered in this study.

Location	Geographical coordinates	Water depth (m)	Distance from shore (m)	Period of measurements
Hopa	41°25′24″N, 41°23′00″E	100	4600	01 January 1996–31 December 1996
Sinop	42°07′24″N, 35°05′12″E	100	11600	01 January 1996–30 June 1996
Gelendzhik	44°30′27″N, 37°58′42″E	85	7000	01 July 1996–31 December 1996

Table 3
The used grid definitions in this study and the recommended choices for computational grid discretization in SWAN (Van der Westhuysen, 2002; Akpınar, 2012).

Component	Recommended choices	The used grid definitions in this study
Directional resolution ($\Delta\theta$)		
Wind sea conditions	15–10°	10°
Swell conditions	5–2°	–
Frequency resolution ($\Delta\sigma/\sigma$)	0.1	0.09
Frequency range (f)		
Minimum	0.04 Hz	0.04 Hz
Maximum	1.00 Hz	1.00 Hz
Spatial resolution (Δx, Δy)		
Open seas conditions	2 km × 2 km	1.3 km × 1.8 km
Shallow water conditions	1000–100 m	–
For harbour condition	20–50 m	–

the Sinop and Gelendzhik buoy stations. All buoy locations are exposed to open sea. Some basic features of buoy stations, their locations and measurements periods are given in Table 2. The detailed information on the wave measurements at these stations is described in Özhan et al. (1995).

The minimum, maximum, and average values of the observed significant wave height (H_{m0}) and average wave period (T_{m02}) at Hopa station during the considering time period in this study are 0.03, 4.10, and 0.58 m (2.1, 8.9, and 4.0 s), respectively. They are 0.07, 3.45, and 0.80 m (1.9, 7.4, and 3.8 s) at Sinop station and 0.07, 4.82, and 1.02 m (1.9, 8.2, and 3.9 s) at Gelendzhik station. The mean observed mean wave directions at Hopa and Sinop buoys are 272° and 204°, respectively. However, these values for both stations do not give any information on the dominant direction which is the direction of the most energetic wave in the spectrum. There are gaps in the records. The performance of the developed SWAN model was assessed with scatter diagrams (see Fig. 12) showing relationships between concurrent simulated and observed wave parameters as well as the temporal variations of the simulated and observed data.

3.4. Bathymetry

The bathymetry area spans the region between 40° N and 48° N, and 27° E and 42° E and includes the Seas of Marmara and Azov. The bathymetry data for the Black Sea were provided from the National Geophysical Data Center by the National Oceanic and Atmospheric Administration (NOAA). The spatial resolution of the bathymetry data source is 0.0167° × 0.0167° and the bathymetry is shown in Fig. 1. In other words, it represents a spatial resolution of 1.3 km × 1.8 km as can be seen in Table 3. These data were interpolated to the model grid by applying the Kriging method, which is a geostatistical technique to interpolate the unknown values from data observed at known adjacent locations (Krige, 1951), and then adapted to the wave model requirements. Application of the Kriging method requires two steps which are firstly the determination of variogram function to express the spatial variation, and secondly the fitting of a theoretical variogram function (Matheron, 1963). This technique has been found a wide application area from mining to hydrology (Journel and Huijbregts, 1978; Isaaks and Srivastava, 1989).

4. Set-up of SWAN wave model

4.1. Grid information and choice of source terms

In this study, SWAN cycle III version 40.85 was used for the wave simulations. The model was executed in third generation and non-stationary mode with spherical coordinates. Both linear and exponential wind input growths were included in the model. The formulation for wind input parameterization developed by Komen et al. (1984) for the exponential growth of wind input was used since it has been revealed by Moeini et al. (2010) that this expression leads to a more accurate hindcast of significant wave height. Dissipation due to depth-induced wave breaking is treated by the Battjes and Janssen (1978) spectral formulation with $\alpha=1$ and $\gamma=0.73$, bottom friction is modelled using the JONSWAP form with a friction coefficient of $C_{bottom}=0.067$ m^2 s^{-3}, and the Komen et al. (1984) formulation for whitecapping is applied with $C_{ds}=2.36\times10^{-5}$, and the steepness dependence was chosen following Rogers et al. (2003) by choosing $\delta=1$ (See SWAN technical manual, SWAN team, 2012). Quadruplet and triad-wave interactions were activated using the default settings for the DIA (Hasselmann et al., 1985) and the LTA (Eldeberky, 1996). Formulations of available physical processes and their associated coefficients included in the model are summarized in Table 4.

The SWAN model was set up to cover the Black Sea from the longitude 27° East to 42° East and for the latitude from 40° North to 48° North with a fine grid resolution (1.3 km × 1.83 km) of 0.0167° by 0.0167°, what gives 901 points for the longitude and 481 points for the latitude. The grid includes 190,687 sea points which is 44% of the total number of grid points, where calculation is performed and output values are generated. The number of frequencies used to describe the wave spectrum is 35 and the number of directions in the 360° rose is 36, and the lowest and highest frequencies equal to 0.04 and 1 Hz, respectively. This means that the periods of simulated wave were between 1 and 25 s covering typical surface waves in the Black Sea. The temporal resolution was 6 h and 30 min for wind inputs and internal time stepping, respectively. The recommended choices and the used grid definitions in this study for computational grid discretization in the SWAN model are summarized in Table 3.

Before the full hindcast with the SWAN model was carried out, a few sensitivity tests analyses were performed to obtain optimal model settings. Sensitivity tests for only post-processing were carried out for the internal time step, frequency interval, frequency and direction resolution, and integration range for output variables. From these analyses, it was understood that

Table 4
Formulations of available physical processes and their associated coefficients included in the model for application of the model.

Physical process	Formulation	Coefficients
Linear wave growth	Cavaleri and Malanotte-Rizzoli (1981) and Tolman (1999)	
Exponential wave growth	Komen et al. (1984)	
Whitecapping	Hasselmann (1974) and WAMDI Group (1988)	$C_{ds}=2.36\times10^{-5}$ $\delta=0$ $p=4$ $S_{PM}=3.02\times10^{-3}$
Quadruplet wave–wave interactions	Hasselmann et al. (1985)	$\lambda=0.25$ $C_{n/4}=3\times10^{7}$ $C_{sh1}=5.5$ $C_{sh2}=6/7$ $C_{sh3}=-1.25$
Bottom friction	Hasselmann et al. (1973)	$C_{JON}=0.067$ m^2 s^{-3}
Triad wave–wave interactions	Eldeberky (1996)	$\alpha_{EB}=0.1$
Depth-induced wave breaking	Battjes and Janssen (1978)	$\alpha_{BJ}=1$ $\gamma_{BJ}=0.73$

frequency interval, frequency, and direction resolution had almost no impact on the computational results. Therefore, only results of the sensitivity analyses carried out for the internal time step and integration range are presented in the following section.

4.2. Sensitivity analysis for time step

To decide which time step is required for the final computations, the SWAN model was run for a test period of 1-month, we chose December 1995 as it experienced some storm events. The time step should be small enough to catch the effect of relatively fast temporal changes in wind speed and direction on the wave field but large enough to make the computation practically feasible. The computations were performed for five different temporal resolutions and output results were obtained for Hopa and Sinop buoy stations. The SWAN output parameters are the significant wave height (H_{m0}), mean wave direction (DIR or θ), and the spectral periods (T_{m01}, T_{m02} and $T_{m\text{-}1,0}$) which are based on ratios of the zeroth-moment m_0 with the frequency moments m_1, m_2 and $m_{\text{-}1}$ respectively. In addition the directional spreading of the waves, and the normalized frequency width of the spectrum as defined by Battjes and Van Vledder (1984) were computed and used in the sensitivity analysis. The simulations were carried out on 6 core Intel Xeon processor with a speed of 3.2 GHz and 12 GByte internal memory. A computation for 1 month with a time step of 30 min took a simulation time of about 8 h. The results were presented as the temporal variations of different wind and wave parameters in Figs. 5 and 6. As can be seen from the figures, the results show more pronounced dynamic behaviour as the time step becomes smaller. A reduction of the time step from 30 to 15 min only slightly changed the results. As the differences are sufficiently small we consider a time step of 30 min sufficient for the full wave hindcast.

4.3. Sensitivity of integration range

A property of the SWAN model is that integral output parameters are based on integration over the full frequency range, supplemented with a contribution from the f^{-4} parametric tail (SWAN team, 2012). In practise, this implies that the integration range stretches from 0.04 to 10 Hz (the upper frequency of the parametric tail in the SWAN model). Integral wave parameters based on buoy data are usually given for a much smaller frequency interval, typically in the range between 0.5 and 1 Hz, depending on the type of buoy. This mismatch in integration range can easily lead to significant differences in parameters values, leading to incorrect conclusions about model performance. It is therefore crucial that integral wave parameters used in the buoy-model comparison are based on integration over the same frequency interval. The results of these analyses at two different buoy stations are shown in Figs. 7 and 8. The sensitivity analysis of the integration range shows that care must be taken in comparing buoy data with wave model data. The example also shows that, depending on the wave conditions, the results can be much different. The test of integration range shows that the difference becomes smaller as the waves and periods are higher. It is also seen that H_{m0} is rather insensitive to the integration range, and T_{m01} is less sensitive than T_{m02}. Consequently, we stress

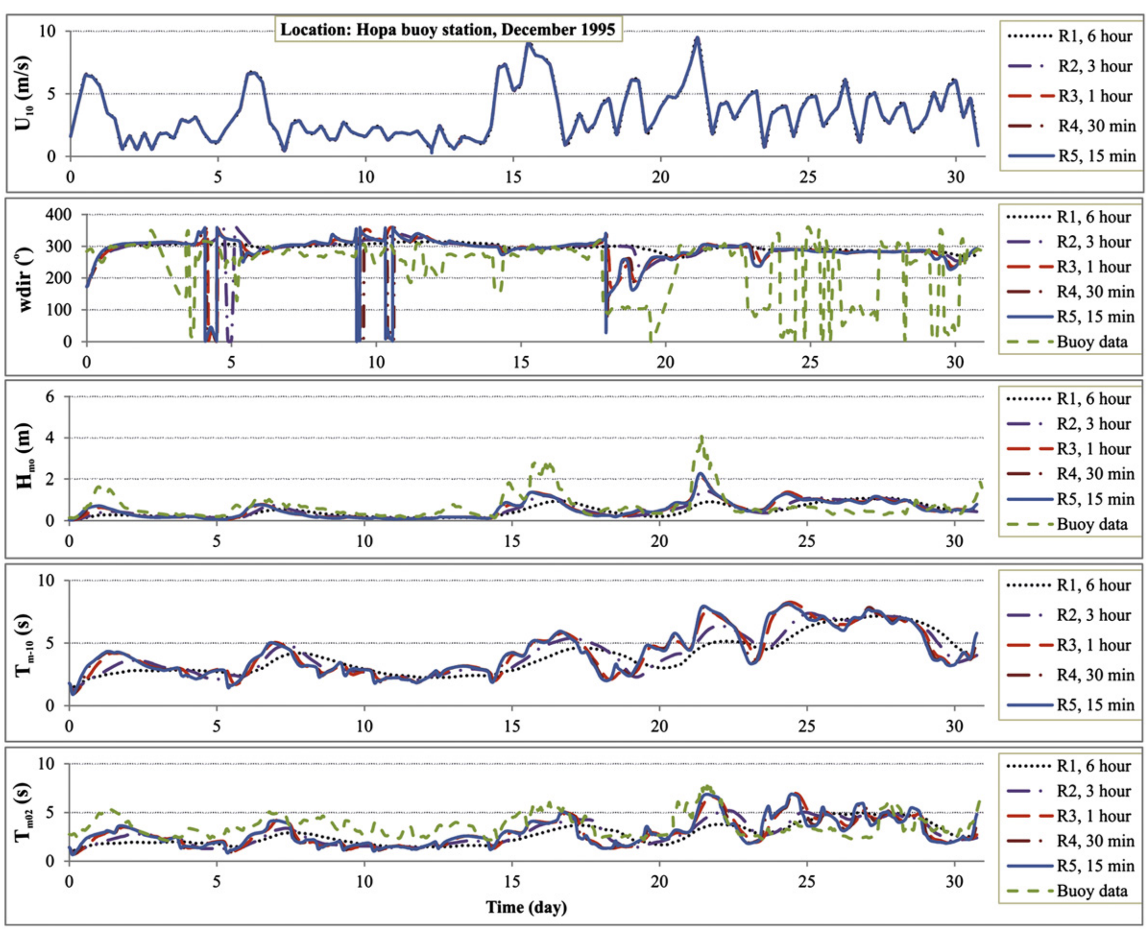

Fig. 5. Comparison of the results obtained for sensitivity analysis of time step at Hopa buoy station for December 1995.

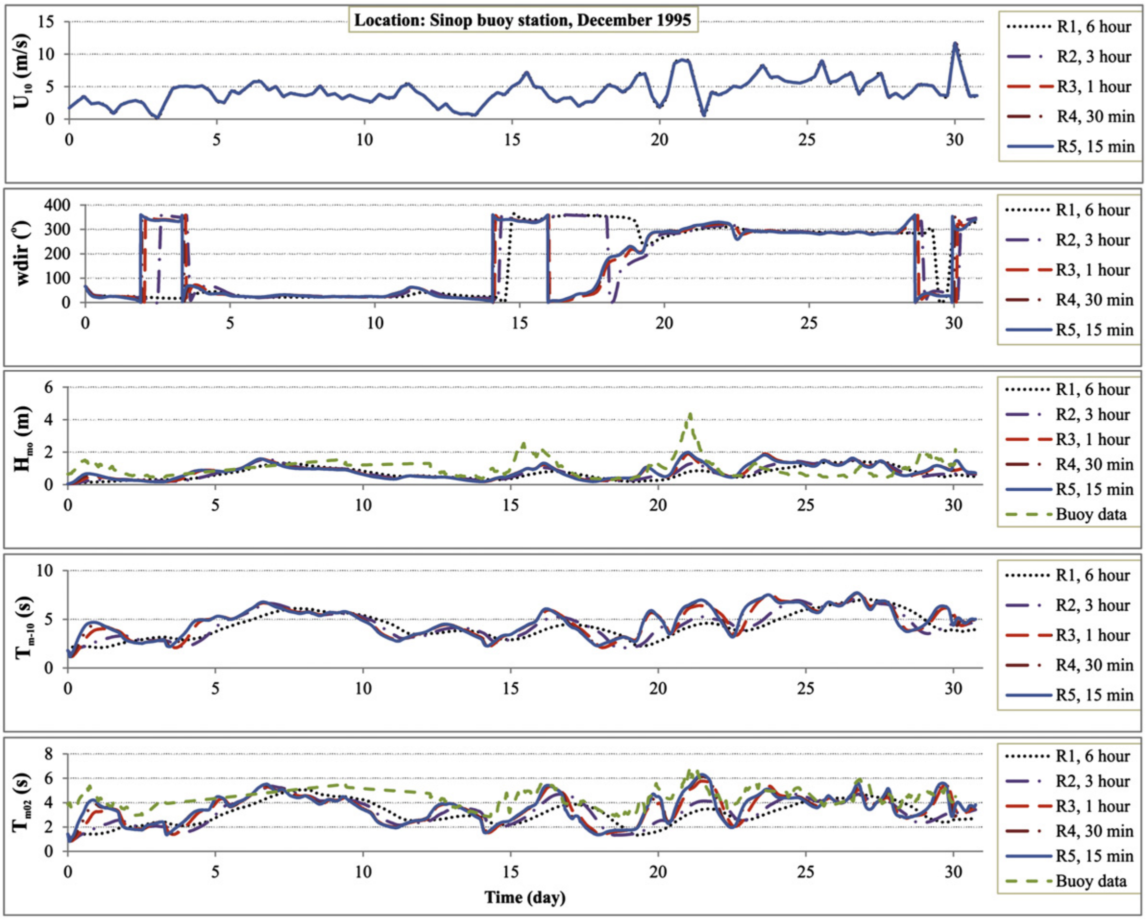

Fig. 6. Comparison of the results obtained for sensitivity analysis of time step at Sinop buoy station for December 1995.

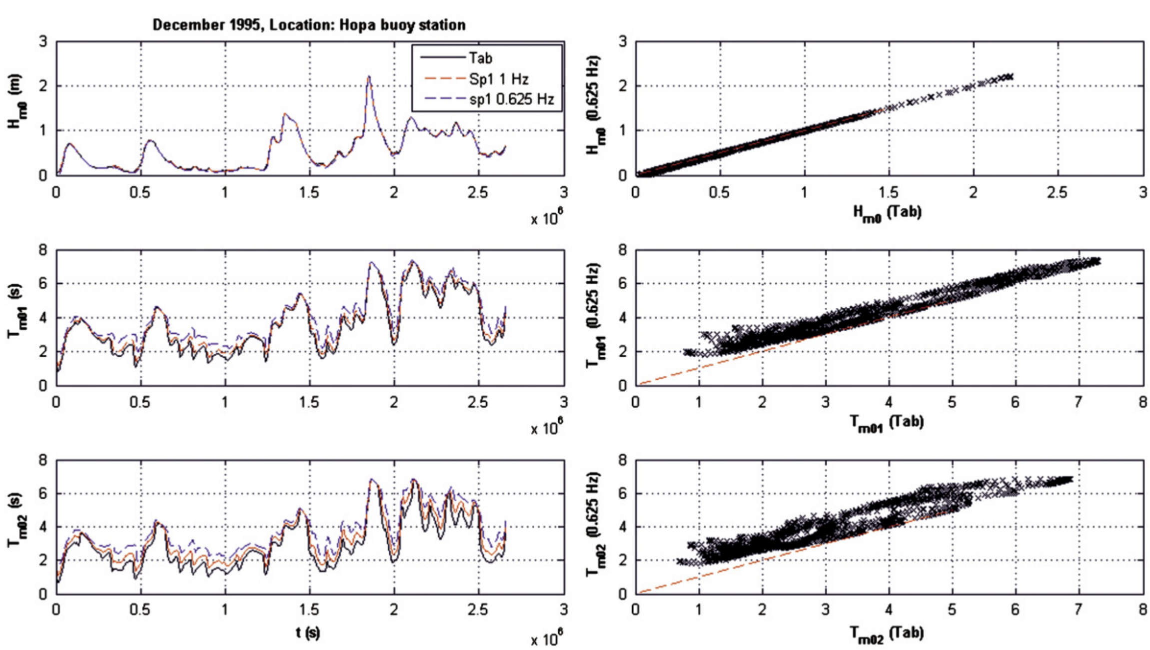

Fig. 7. Comparison of the results obtained for sensitivity analysis of integration range at Hopa buoy station for December 1995.

that the differences for H_{m0} are negligible, small for T_{m01}, and large for T_{m02} (as this is strongly influenced by the upper frequencies). This sensitivity analysis can be an argument/advise to use other more robust/representative wave period parameters for comparison and model performance assessment, such as the $T_{m-1,0}$. For the present study we computed the integral wave parameters over the

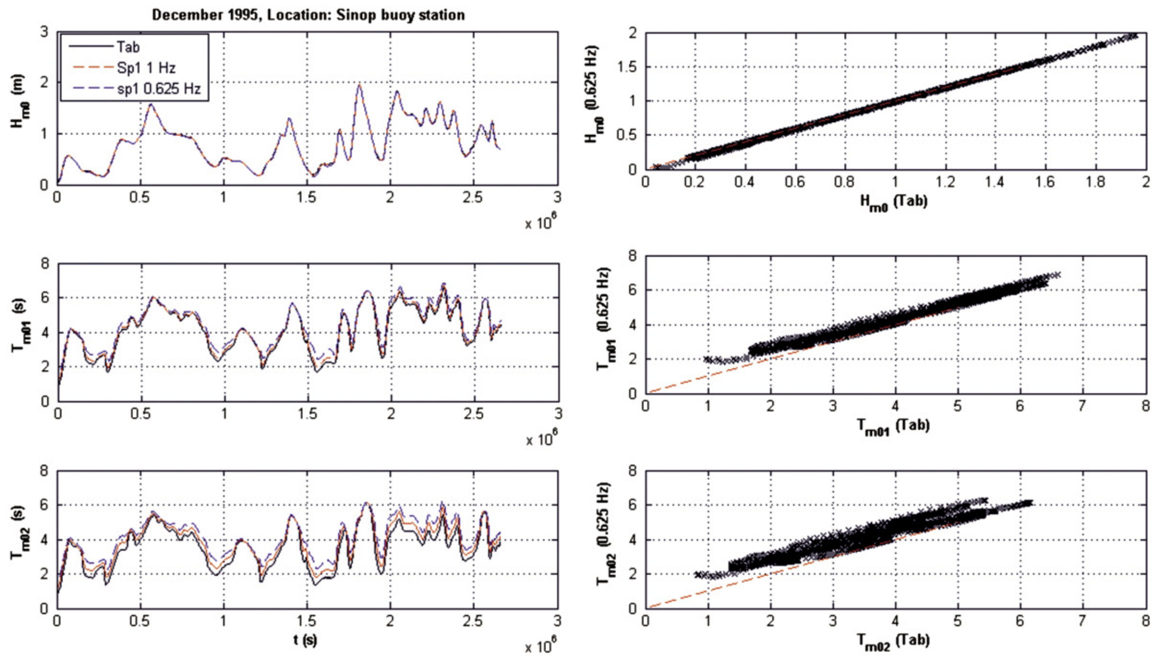

Fig. 8. Comparison of the results obtained for sensitivity analysis of integration range at Sinop buoy station for December 1995.

frequency interval from 0.04 to 0.625 Hz, which has also been used in the analysis of the buoy data.

5. Results and discussion

5.1. Error measuring criteria

For quantitative evaluation of the degree of accuracy of the model results, bias parameter, root mean square error (RMSE), the scatter index (SI), correlation coefficient (R), mean absolute error (MAE), and determination coefficient (R^2) were used for comparison of measured and predicted values. These statistical parameters were calculated as follows:

$$\text{bias} = \sum_{i=1}^{N} \frac{1}{N}(P_i - O_i) \tag{17}$$

$$\text{RMSE} = \sqrt{\frac{1}{N}\sum_{i=1}^{N}(P_i - O_i)^2} \tag{18}$$

$$\text{SI} = \frac{\text{RMSE}}{\frac{1}{N}\sum_{i=1}^{N} O_i} \tag{19}$$

$$R = \frac{\sum_{i=1}^{N}((P_i-\overline{P})(O_i-\overline{O}))}{\sqrt{(\sum_{i=1}^{N}(P_i-\overline{P})^2)(\sum_{i=1}^{N}(O_i-\overline{O})^2)}} \tag{20}$$

$$\text{MAE} = \frac{\sum_{i=1}^{N}\Delta\theta_{O,P}}{N} \tag{21}$$

where O_i is the observed value, $\overline{O}$ is the mean value of the observed data, P_i is the predicted value, $\overline{P}$ is the mean value of the predicted data, and N is the number of data. The shortest distance $\Delta\theta_{1,2}$ between two directions is computed as: $\Delta\,\theta_{1,2} = 180 - |180 - |\theta_1 - \theta_2||$. Mean directions are computed on the basis of the mean of their component in two orthogonal directions.

5.2. Validation of SWAN hindcasts against buoy data

The results of full wave hindcast with a frequency interval of 0.04–0.625 Hz and 30 min of internal time step for selected periods were compared with measured buoy data at three locations. Figs. 9–11 show a comparison between data measured for the NATO TU-WAVES project and simulated by the SWAN model at the three locations: Hopa, Sinop, and Gelendzhik, respectively. Three examples of temporal variations of four wave parameters: significant wave height (H_{m0}), mean wave direction (DIR), nautical convention, average spectral wave period (T_{m02}), and spectral mean period (T_{m01}) are shown in these figures. The comparison of the measured and simulated significant wave heights reveals that H_{m0} (bias $= -0.18$ m at Hopa, bias $= -0.32$ m at Sinop, and bias $= -0.35$ m at Gelendzhik) is reasonably reproduced by the SWAN model for all stations as can be seen from Figs. 9–11. The SWAN model with its present settings captures the peaks and troughs of the temporal variations of significant wave height and average wave period (T_{m02}) very well. However, it has less accurate estimates for the maximum values of the both parameters. This underestimation of the peaks may be related to the rather course temporal and spatial resolutions of the ECMWF wind fields; see, e.g. Cavaleri (2009) for a discussion on this topic. These data, with about 0.25° of spatial resolution and 6 hourly fields are still very coarse for the Black Sea. This negative bias in wave parameters is also probably due to low wind speeds fields produced by the meteorological models of the ECMWF, which is probably affected by orographic effects in the ECMWF wind fields. The orography is rather complicated by the mountains presence in the most of Black Sea surrounding land areas: Balkans on its West side, high Caucasus ridges in the east and Pontean mountainsides in the northern Turkey. Besides the aforementioned features of geographic location, bathymetry and orography complexity of the shores, the climate over the Black Sea and adjoining land regions is affected by the atmospheric circulation conditions over the basin; see Cherneva et al. (2008) for a description of the orographic effects on the Black Sea. This situation resulted in different accuracies of the model results at various stations.

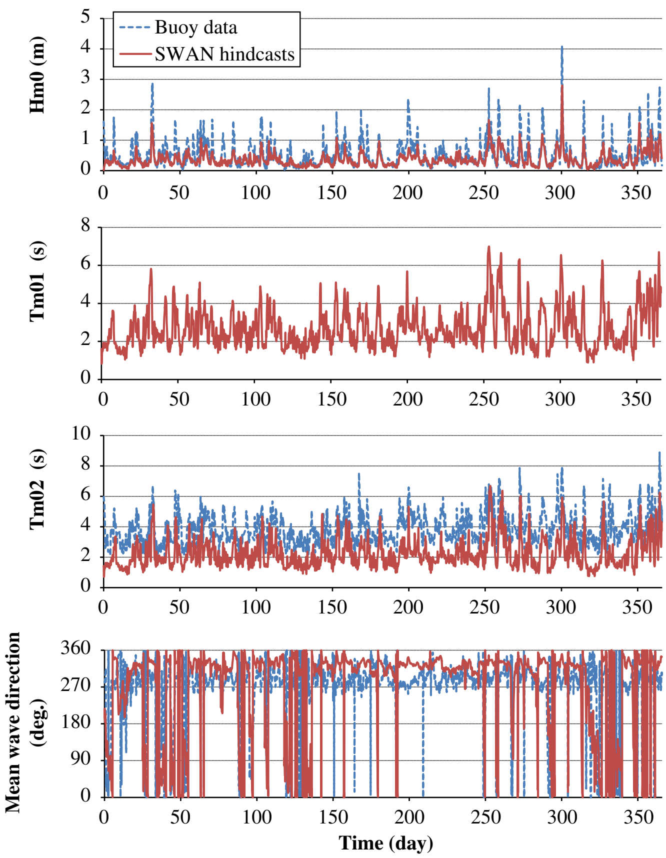

Fig. 9. Temporal variations of the hindcasted and observed wave parameters at the Hopa buoy station (for all months of 1996 year).

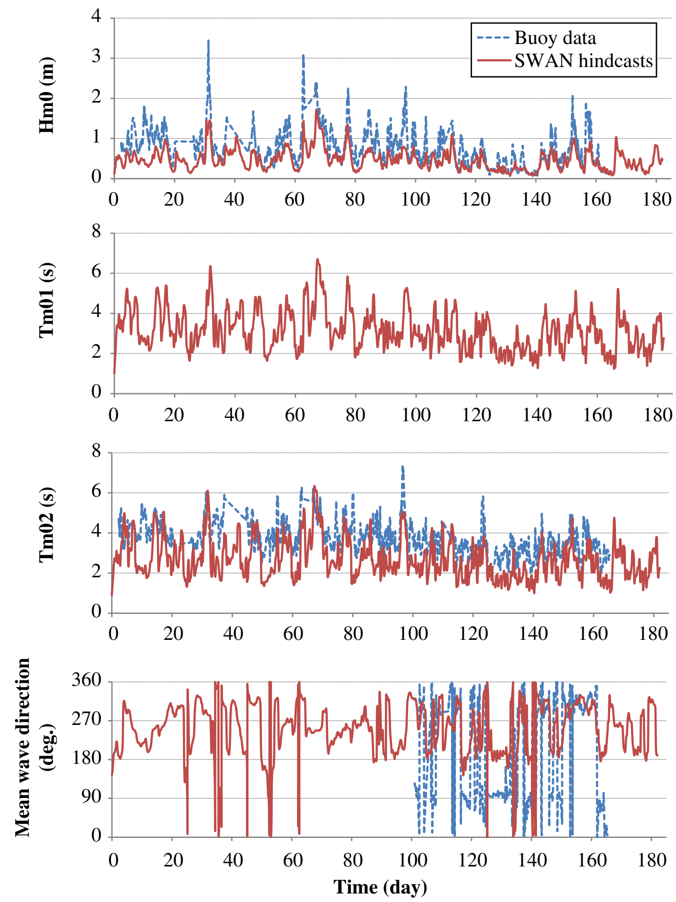

Fig. 10. Temporal variations of the hindcasted and observed wave parameters at the Sinop buoy station (for the first 6 months of 1996).

The SWAN model outputs have a temporal resolution of 30 min. The simulated time series for 30-min resolution were obtained at the buoy locations by bi-linear interpolation in the spectral components of the four surrounding nearest grid points. However, there are gaps in the measured records due to various causes of malfunctioning. Therefore, for quantitative evaluation of the model performance, concurrent data were obtained from the measured and simulated wave records for each station. Figs. 12–14 show the scatter plots of concurrent simulated and observed significant wave height, for all the available data of 1996 at three stations (Hopa, Sinop, and Gelendzhik). The basic statistical parameters and error measures are also listed next to the graphs. A reasonable agreement (R=0.83 at Hopa buoy, R=0.82 at Sinop buoy, and R=0.86 at Gelendzhik buoy) was obtained for the significant wave height in terms of error measures (e.g. bias parameter and correlation coefficient) at three stations. While the bias parameter is 0.18 m at the Hopa station, it is 0.32 and 0.35 m for the Sinop and Gelendzhik stations, respectively. Correlation coefficients vary from 0.82 at Sinop location to 0.83 at Hopa location to 0.86 at Gelendzhik station. From this, it can be stated that the SWAN model estimations for Gelendzhik station are more accurate than that of the other two stations, and also, the hindcasts for Hopa station are better than that of Sinop station. SWAN model underestimated the observed values of H_s at all the locations analysed. The correlation coefficients between the observed and simulated significant wave height are higher than those of average wave periods (T_{m02}) and directions at all buoy stations. As can be seen in Tables 5–7, the higher negative bias parameter in the prediction of the average wave period (T_{m02}) at all stations means that the SWAN model slightly underestimates the average wave period (T_{m02}). On the other hand, it can be seen from Tables 5–7 that the root mean square errors of the SWAN model for average wave period (T_{m02}) and mean direction are high but the SWAN model has low error in the prediction of the significant wave height.

Here, the findings of our SWAN modelling (R^2=0.67 and SI=0.56 for H_{m0} and R^2=0.42 and SI=0.35 for T_{m02}) are generally in agreement with the results of Lin et al. (2002) (R^2=0.51 and SI=0.57 for H_{m0} and R^2=0.12 and SI=0.38 for T_p) and Moeini and Etemad-shahidi (2009) (R^2=0.83 and SI=0.24 for H_{m0} and R^2=0.48 and SI=0.16 for T_p) that used the SWAN model for wave simulation in the Chesapeake Bay and Lake Erie, respectively. They obtained a slight underestimation in the prediction of the wave parameters for the simulated periods.

The monthly variations of RMSE, bias, and R^2 values for wave parameters are shown in Tables 5–7. At the Hopa station, RMSE value ranges from 0.20 to 0.51 m, 1.5 to 2.1 s, and 37–145° for H_{m0}, T_{m02}, and DIR, respectively, bias parameter from −0.08 to −0.28 m, −1.36 to −2.00 s, and −52° to 35° for H_{m0}, T_{m02}, and DIR, respectively, and R^2 value from 0.23 to 0.93, 0.16 to 0.81, and 0.01 to 0.35 for H_{m0}, T_{m02}, and DIR, respectively. The performance of the SWAN model is well enough in terms of RMSE, bias, and R^2 values for H_{m0} at the Sinop and Gelendzhik stations. In general, results for significant wave height (H_{m0}) are satisfactory for every month of the year. However, validations of simulated mean wave period (T_{m02}) and direction are not satisfactory for every month of the year.

This validated regional wave model constitutes the basis for developing a wave climate study in the region. In this sense, some encouraging preliminary results were obtained. Finally it is central to stress the importance and need of more in situ wave observations along the north and south coasts of the Black Sea to allow more and better scientific studies leading to appropriate knowledge of this important phenomenon.

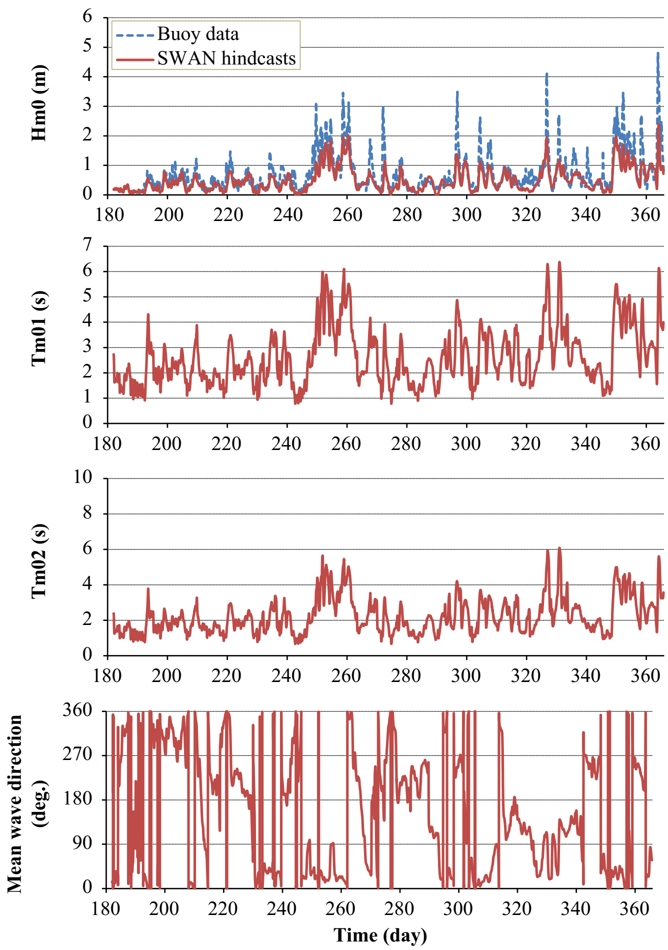

Fig. 11. Temporal variations of the hindcasted and observed wave parameters at the Gelendzhik buoy station (for the last 6 months of 1996).

5.3. Comparison of SWAN hindcasts with JONSWAP results

This section discusses the performance of the developed SWAN model in comparison with the parametric JONSWAP method. This method used the ERA-Interim atmospheric model wind data at the closest grid points to the Hopa and Sinop buoy stations in the wind fields that were also used as inputs for the SWAN model. As the wind data were only available at 6 hourly intervals, we could not get more accurate estimates of wind speed and direction as suggested in the discussion of Eqs. (2) and (3). Figs. 15 and 16 show scatter diagrams regarding the results of JONSWAP method and the basic statistical parameters, and error measures are listed next to the graphs. The results of the JONSWAP method show that more accurate wave heights are obtained at Sinop station (R=0.44 for H_{m0}) that at Hopa station (R=0.31 for H_{m0}).

The summary of statistical analysis of wave prediction errors considering the same time period is shown in Table 8. As can be seen from the table, according to all error indices, the accuracy of the SWAN model for all wave parameters is far better than that of the JONSWAP method. The scatter indices of the SWAN model at Hopa station are about 0.63 and 0.45 for the prediction of H_{m0} and T_{m02}, respectively, while these indices at Sinop station are about 0.56 and 0.35 for the estimation of H_{m0} and T_{m02}, respectively. The scatter indices of the JONSWAP method are about 1.08, 0.70 and 0.73, 0.54 for the prediction of H_{m0} and T_{m02} at Hopa and Sinop station, respectively. As seen in Table 8, the accuracy of the SWAN model for the predictions of H_{m0} and T_{m02} is higher at Sinop station in comparison to Hopa station, while the accuracy of the SWAN model in the estimation of mean wave direction is higher at the Hopa station.

5.4. Comparison of SWAN hindcasts with the results of the previous studies

The SWAN model results were also compared with the METU3 hindcasts, which were the products of a wave modelling work conducted by Abdalla et al. (1995). Unfortunately, only a 1-month wave record at the Hopa buoy station was available. The METU3

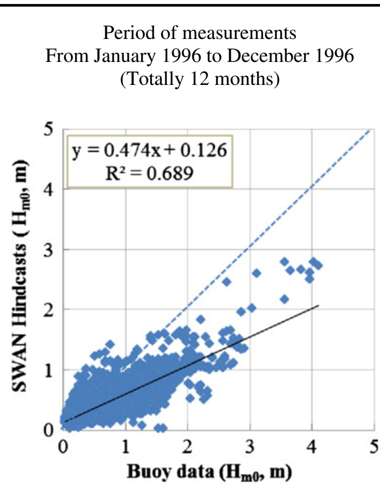

Significant wave height	Buoy data	SWAN Hindcast
Number of data	3205	17568
Minimum value (m)	0.03	0.02
Maximum value (m)	4.10	2.80
Mean value (m)	0.58	0.37
Standard deviation (m)	0.52	0.25
Concurrent data		
Number of data	3197	
Bias (m)	-0.18	
Correlation coefficient	0.83	
RMSE (m)	0.37	
Scatter index	0.63	

Fig. 12. Scatter plot of measured buoy data against simulated SWAN hindcasts at the Hopa buoy station (left) and basic statistical parameters (right).

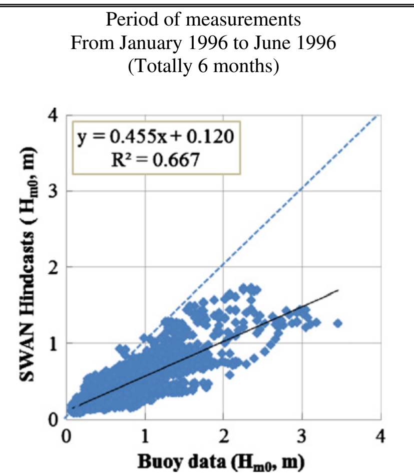

Significant wave height	Buoy data	SWAN Hindcast
Number of data	2523	8742
Minimum value (m)	0.07	0.08
Maximum value (m)	3.45	1.72
Mean value (m)	0.80	0.47
Standard deviation (m)	0.50	0.26
Concurrent data		
Number of data	2522	
Bias (m)	-0.32	
Correlation coefficient	0.82	
RMSE (m)	0.45	
Scatter index	0.56	

Fig. 13. Scatter plot of measured buoy data against simulated SWAN hindcasts at the Sinop buoy station (left) and basic statistical parameters (right).

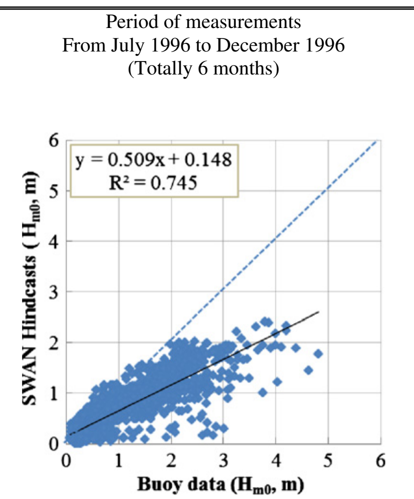

Significant wave height	Buoy data	SWAN Hindcast
Number of data	1649	8826
Minimum value (m)	0.07	0.01
Maximum value (m)	4.82	2.41
Mean value (m)	1.02	0.50
Standard deviation (m)	0.83	0.40
Concurrent data		
Number of data	1642	
Bias (m)	-0.35	
Correlation coefficient	0.86	
RMSE (m)	0.60	
Scatter index	0.58	

Fig. 14. Scatter plot of measured buoy data against simulated SWAN hindcasts at the Gelendzhik buoy station (left) and basic statistical parameters (right).

Table 5
Monthly root mean square error (RMSE), bias, and determination coefficient (R^2) between concurrent simulated data by the SWAN model and observed wave parameters at the Hopa buoy station for all months of 1996 year.

Month	The number of concurrent data	RMSE (m, s, °) H_{m0}, T_{m02}, DIR	Bias (m, s, °) H_{m0}, T_{m02}, DIR	SI H_{m0}, T_{m02}, DIR	R^2 H_{m0}, T_{m02}, DIR
January	284	0.34, 1.8, 111	−0.23, −1.6, −18	0.68, 0.51,0.42	0.46, 0.25, 0.16
February	293	0.42, 1.6, 126	−0.20, −1.4, −13	0.67, 0.41, 0.54	0.78, 0.63, 0.21
March	309	0.37, 1.7, 80	−0.20, −1.6, −18	0.64, 0.44, 0.29	0.44, 0.36, 0.24
April	241	0.29, 1.8, 99	−0.10, −1.6, −5	0.63, 0.45, 0.35	0.45, 0.37, 0.09
May	319	0.20, 1.6, 145	−0.10, −1.5, −19	0.62, 0.48, 0.53	0.34, 0.16, 0.01
June	342	0.31, 1.8, 64	−0.20, −1.6, 23	0.56, 0.45, 0.22	0.75, 0.34, 0.02
July	237	0.46, 2.1, 57	−0.28, −2.0, 35	0.70, 0.49, 0.20	0.58, 0.50, 0.01
August	228	0.20, 1.9, 37	−0.08, −1.8, 27	0.50, 0.50, 0.13	0.23, 0.25, 0.04
September	247	0.43, 1.8, 70	−0.22, −1.6, 22	0.50, 0.38, 0.25	0.72, 0.62, 0.35
October	210	0.41, 2.0, 83	−0.22, −2.0, 26	0.50, 0.45, 0.30	0.93, 0.81, 0.12
November	215	0.36, 2.0, 140	−0.09, −1.8, −52	0.80, 0.50, 0.52	0.70, 0.62, 0.08
December	272	0.51, 1.9, 118	−0.21, −1.7, 15	0.64, 0.42, 0.48	0.57, 0.65, 0.20

Table 6
Monthly root mean square error (RMSE), bias, and determination coefficient (R^2) between concurrent simulated data by the SWAN model and observed wave parameters at the Sinop buoy station for the first 6 months of 1996.

Month	The number of concurrent data	RMSE (m, s, °) H_{m0}, T_{m02}, DIR	Bias (m, s, °) H_{m0}, T_{m02}, DIR	SI H_{m0}, T_{m02}, DIR	R^2 H_{m0}, T_{m02}, DIR
January	380	0.54, 1.5, n.d.	−0.46, −1.1, n.d.	0.57, 0.36, n.d.	0.30, 0.03, n.d.
February	403	0.48, 1.4, n.d.	−0.33, −1.1, n.d.	0.55, 0.35, n.d.	0.72, 0.33, n.d.
March	498	0.53, 1.4, n.d.	−0.39, −1.1, n.d.	0.52, 0.35, n.d.	0.70, 0.39, n.d.
April	532	0.43, 1.2, 127	−0.32, −1.1, 61	0.56, 0.33, 0.64	0.54, 0.58, 0.18
May	478	0.22, 1.1, 125	−0.13, −1.0, 63	0.48, 0.35, 0.69	0.67, 0.37, 0.18
June	231	0.41, 1.1, 82	−0.29, −1.0, 27	0.54, 0.32, 0.32	0.86, 0.64, 0.70

n.d., n o measured data.

Table 7
Monthly root mean square error (RMSE), bias, and determination coefficient (R^2) between concurrent simulated data by the SWAN model and observed wave parameters at the Gelendzhik buoy station for the last 6 months of 1996.

Month	The number of concurrent data	RMSE (m, s, °) H_{m0}, T_{m02}, DIR	Bias (m, s, °) H_{m0}, T_{m02}, DIR	SI H_{m0}, T_{m02}, DIR	R^2 H_{m0}, T_{m02}, DIR
July	175	0.20, 1.4, n.d.	−0.13, −1.3, n.d.	0.42, 0.46, n.d.	0.58, 0.27, n.d.
August	234	0.27, 1.5, n.d.	−0.14, −1.3, n.d.	0.55, 0.47, n.d.	0.43, 0.29, n.d.
September	364	0.72, 1.5, n.d.	−0.50, −1.3, n.d.	0.51, 0.33, n.d.	0.64, 0.70, n.d.
October	257	0.49, 1.6, n.d.	−0.26, −1.4, n.d.	0.66, 0.45, n.d.	0.80, 0.51, n.d.
November	268	0.53, 1.5, n.d.	−0.30, −1.2, n.d.	0.55, 0.36, n.d.	0.76, 0.38, n.d.
December	344	0.82, 1.6, n.d.	−0.57, −1.3, n.d.	0.55, 0.35, n.d.	0.67, 0.53, n.d.

n.d., no measured data.

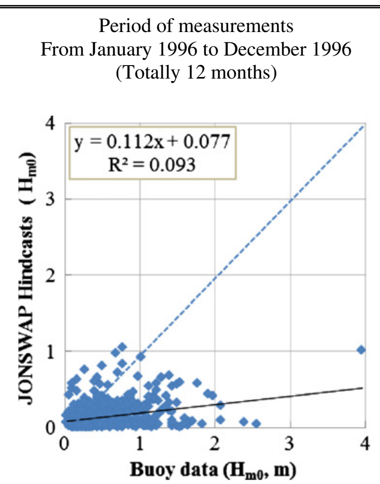

Significant wave height	Buoy data	JONSWAP Hindcast
Number of data	3205	826
Minimum value (m)	0.03	0.00
Maximum value (m)	4.10	1.06
Mean value (m)	0.58	0.13
Standard deviation (m)	0.52	0.15
Concurrent data		
Number of data	671	
Bias (m)	-0.37	
Correlation coefficient	0.31	
RMSE (m)	0.54	
Scatter index	1.08	

Fig. 15. Scatter plot of measured buoy data against hindcasted JONSWAP results at the Hopa buoy station (left) and basic statistical parameters (right).

results were obtained by using the ECMWF analysis surface wind fields produced by the operational meteorological model of the ECMWF. Appropriate assessments have been made by superposing the temporal pattern of the simulated SWAN predictions and the obtained METU3 hindcasts during January 1995 (Fig. 17). The temporal pattern of the SWAN model results is similar to buoy measuring data as can be seen from this figure. The SWAN model also has better estimates of the peak and trough values compared to the METU3 hindcasts in the time series of significant wave height. In addition, appropriate evaluations have been done by comparing the error statistics of the WAM Cycle 4 model results of Cherneva et al. (2008), which is a model validation study for three different time periods at three locations in the Black Sea, and our SWAN hindcasts obtained during September 1–November 30, 1996, at Gelendzhik station, 21–28 January, 1995, at Hopa station, and November 1994 at Sinop station (Table 9). As can be seen from the table, correlations between measured data and the SWAN hindcasts for both wave parameters at all buoy stations are much better than correlations between measured data and the WAM Cycle 4 results of Cherneva et al. (2008). We therefore conclude that applying SWAN is a good step in producing more accurate wave forecasts in the Black Sea. Besides, there are also a few studies focusing the Black Sea for various purposes as wave energy assessment (Rusu, 2009), oil spills propagation (Rusu, 2010a), modelling wind waves (Rusu and Ivan, 2010), and wave-current interaction (Rusu, 2010b). Rusu (2010a) has no data available for the comparison and we do not have any

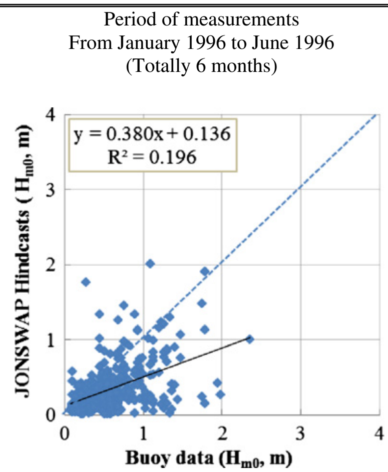

Significant wave height	Buoy data	JONSWAP Hindcast
Number of data	2523	381
Minimum value (m)	0.09	0.01
Maximum value (m)	3.45	2.29
Mean value (m)	0.80	0.39
Standard deviation (m)	0.50	0.36
Concurrent data		
Number of data	289	
Bias (m)	-0.27	
Correlation coefficient	0.44	
RMSE (m)	0.47	
Scatter index	0.73	

Fig. 16. Scatter plot of measured buoy data against hindcasted JONSWAP results at the Sinop buoy station (left) and basic statistical parameters (right).

Table 8
The summary of statistical analysis of models performances during the considering time period at the Hopa and Sinop stations.

		Hopa station		Sinop station	
		SWAN model	JONSWAP model	SWAN model	JONSWAP model
H_{m0}	Bias (m)	−0.18	−0.37	−0.32	−0.27
	Scatter index	0.63	1.08	0.56	0.73
	Correlation coefficient	0.83	0.31	0.82	0.44
T_{m02}	Bias (s)	−1.66	−2.36	−1.06	−0.60
	Scatter index	0.45	0.70	0.35	0.54
	Correlation coefficient	0.75	0.13	0.65	0.03
Direction	Bias (°)	5	–	54	–
	Scatter index	0.37	–	0.57	–
	Correlation coefficient	0.38	–	0.51	–

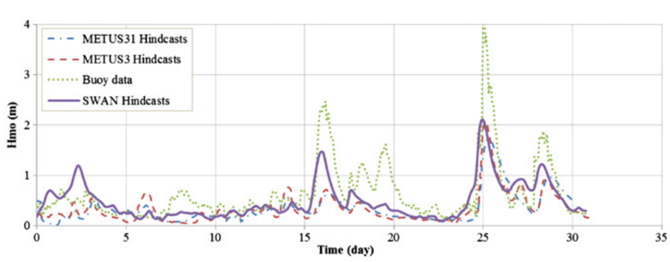

Fig. 17. Comparison of the temporal variations of significant wave height by the SWAN model, buoy data, and METU3 hindcasts (Abdalla et al., 1995) during the whole month of January 1995 at the Hopa station.

comparison with the results of Rusu (2010b) and Rusu and Ivan (2010) because Rusu (2010b) only focussed on the Danube Delta in the Black Sea and while Rusu and Ivan (2010) was used the data of the Gloria drilling unit in the Romanian and Bulgarian coastal areas whereas in this study comparison was possible with the results of Rusu (2009) who concentrates on Gelendzhik and Hopa buoys. Compared with our SWAN hindcasts for H_{m0} Rusu (2009) obtained a slightly higher correlation and lower RMSE (R=0.886 and RMSE=0.364 m), which in our SWAN hindcasts are R=0.863 and RMSE=0.595 m, at the Gelendzhik buoy station and slightly lower correlation and RMSE (R=0.781 and RMSE=0.325 m), which in our SWAN hindcasts are R=0.830 and RMSE=0.366 m, at the Hopa buoy station. However, the statistical error statistics of both hindcast studies at both buoy stations belong to different time periods. They are for time periods between November 1, 1996, and February 6, 1997, at the Gelendzhik and Hopa buoy stations in Rusu (2009), but the time periods of our hindcasts are the last 6 months of 1996 at the Gelendzhik buoy station and all months of 1996 at the Hopa buoy station. Therefore, it is difficult to decide which model performance is better because the models have different time periods in the statistics of the errors. However, it is concluded that both models have good performance.

5.5. Directional dependence

So far, an omni-directional analysis was carried out to assess the performance of the SWAN model in the Black Sea. In view of the close proximity of the measurement buoys to the mountainous coasts, and in view of the fact that the dominant wind direction is from southerly directions, we looked further into directional aspects of the SWAN model performance as this may provide information on systematic errors in the driving wind field and in differences between short and long fetch behaviour. Therefore, in this study, an error analysis was performed to determine whether for southerly winds orographic effect on the wind fields subsequently causes a bias in the wave model results. We have no data for the wave direction at Gelendzhik buoy station and barely data at Sinop buoy station. Therefore, the directional analysis is performed only for the 1996 Hopa buoy data. This is achieved by making a division in two wind direction sectors using the normal to the coast (320°) as a reference. We defined a 180° wind direction sector around it (Fig. 1), to have only offshore winds (winds going to land) at Hopa buoy station. Thus, waves coming from offshore and those coming from land are therefore separated into two populations. Table 10 shows the error statistics or performances of the SWAN model for offshore and land winds. As can be seen, land wind induced waves are less accurate than waves generated by offshore winds. It also appears different performance of the wave model for either type of winds. This suggests that orographic effects may play a role in wave evolution. The wave roses for all winds, offshore winds, and land winds for both measurements and SWAN hindcasts at Hopa buoy station are presented in Fig. 18. It is remarkable that

Table 9
The summary of error statistics of WAM Cycle 4 results of Cherneva et al. (2008) and the SWAN results of this study.

Location	Time period	Parameter	The results of Cherneva et al. (2008)					The results of this study				
			Number of data	R	Bias	RMSE	SI	Number of data	R	Bias	RMSE	SI
Gelendzhik	September 1–November 30, 1996	H_{m0}	690	0.73	0.27	0.53	0.72	889	0.85	−0.37	0.60	0.56
		T_{m02}		0.62	0.22	0.96	0.25		0.74	−1.31	1.52	0.37
Hopa	January 21–Jan 28, 1995	H_{m0}	89	0.75	−0.09	0.75	1.21	102	0.88	−0.25	0.65	0.63
		T_{m02}		0.54	0.15	1.25	0.37		0.93	−0.93	1.19	0.28
Sinop	November 1–November 30. 1994	H_{m0}	245	0.82	−0.28	0.73	0.65	271	0.89	−0.51	0.71	0.50
		T_{m02}		0.75	0.07	0.85	0.20		0.82	−0.74	1.06	0.23

Table 10
The error statistics of the SWAN model for the offshore and land winds.

	H_{m0} (m)			T_{m02} (s)			Wave direction (°)	
	R	RMSE	SI	R	RMSE	SI	MAE	DBIAS
All winds	0.83	0.37	0.63	0.75	1.81	0.45	50.9	34.5
Offshore winds	0.85	0.42	0.60	0.75	1.89	0.44	42.1	36.6
Land winds	0.67	0.25	0.68	0.70	1.68	0.48	66.6	41.1

even for land winds the measured waves are dominated by waves coming from north-westerly directions and that only a small amount of time waves are primarily generated by land winds. A similar characteristic appears in the roses for the SWAN model results, but now there is a markedly directional bias (DBIAS) of about 40° towards the coast. These directional biases in significant wave height, mean wave period and mean wave direction may also be related to the known inaccuracies in third-generation models in so-called slanting fetch effect situations as it seems to be related to the poor role of the DIA in such models, see Ardhuin et al. (2007) for a discussion on this topic. From Fig. 18 it also follows that SWAN seems to over-estimate land wind generated waves for these relative short fetches. Possible sources of error for land wind situations maybe related to inaccuracies in source term balance for short-fetches and to numerical effects. For land winds the fetch is resolved by 5–10 grid points, which may be insufficient to accurately resolve wave growth.

5.6. Shallow water aspects analysis

Despite the fact that the Black Sea is generally a deep basin, it has some shallow areas where shallow water effects may play a role. Information about the location and importance of these processes maybe important for choosing the settings of the SWAN model. If shallow water effects do not play a role, then related source terms may not be activated, thus saving computing time. In this study, we determined the spatial distribution of the magnitude of the physical processes as represented in SWAN to better understand which physical processes (or equivalently SWAN source terms) play a role in deep and shallow water. It is noted that the SWAN source terms are also already an approximation to the true physical processes, but we deem this approach to be a good first step to identify where and to what extent physical processes play a role.

The source term magnitudes S_{mag} are computed as the integral over directions and frequencies of absolute value of each source term. Subsequently, these source term magnitudes are normalized by dividing with the total wave variance m_0, computed as the total integral of the wave variance spectrum $E(f, \theta)$. The reciprocal normalized source term magnitudes can be interpreted as time scales related to the change of wave energy due to a certain physical process, see e.g. Holthuijsen et al. (2008). Thus, we have:

$$S_{mag} = \int_0^{2\pi} \int_{f_{\min}}^{f_{\max}} S(f, \theta) df \, d\theta \tag{22}$$

$$m_0 = \int_0^{2\pi} \int_{f_{\min}}^{f_{\max}} E(f, \theta) df \, d\theta \quad 23)$$

in which f_{min} and f_{max} are the lower and upper limits of the frequency range applied in the SWAN computations, here 0.04 and 1.0 Hz, respectively. The larger the normalized source term magnitude, the more influence a source term (or physical process) has on wave evolution.

For our analysis we selected a severe wave condition in which we expect that shallow water effects will play a role. For our analysis we selected the storm instant of 25 Jan 1995, 00:00 h, characterized by a strong North North-westerly wind in the order of 13.3 m/s. The geographical variation of the normalized source term magnitudes for this storm instant is shown in Fig. 19. The left-hand panels are for the deep water source terms for whitecapping and non-linear four-wave interactions. The right-hand panels are for the surf breaking, bottom friction, and non-linear three-wave interactions.

The variation of the normalized source terms clearly shows that in deep water the processes of wind input, whitecapping dissipation and non-linear four-wave interactions are dominant. Wind and whitecapping are more or less of equal magnitude, where the non-linear four-wave interactions are less strong. Bottom friction becomes important along the shallow edges of the Black Sea, the Sea of Azov and in the north-western part of the Black Sea. This process acts over relatively long distances and may affect wave evolution in this areas, especially for waves coming from the south-east. Surf breaking and triad interactions are only active in the very shallow regions in the Sea of Azov and at some isolated shallow spots along the perimeter of the Black Sea. It is noted that the latter two source terms are usually active in the same shallow areas.

Further insight into the areas where shallow water processes are active was obtained by determining the spatial distribution of the non-dimensional parameter (H_{m0}/d). Fig. 20 shows the

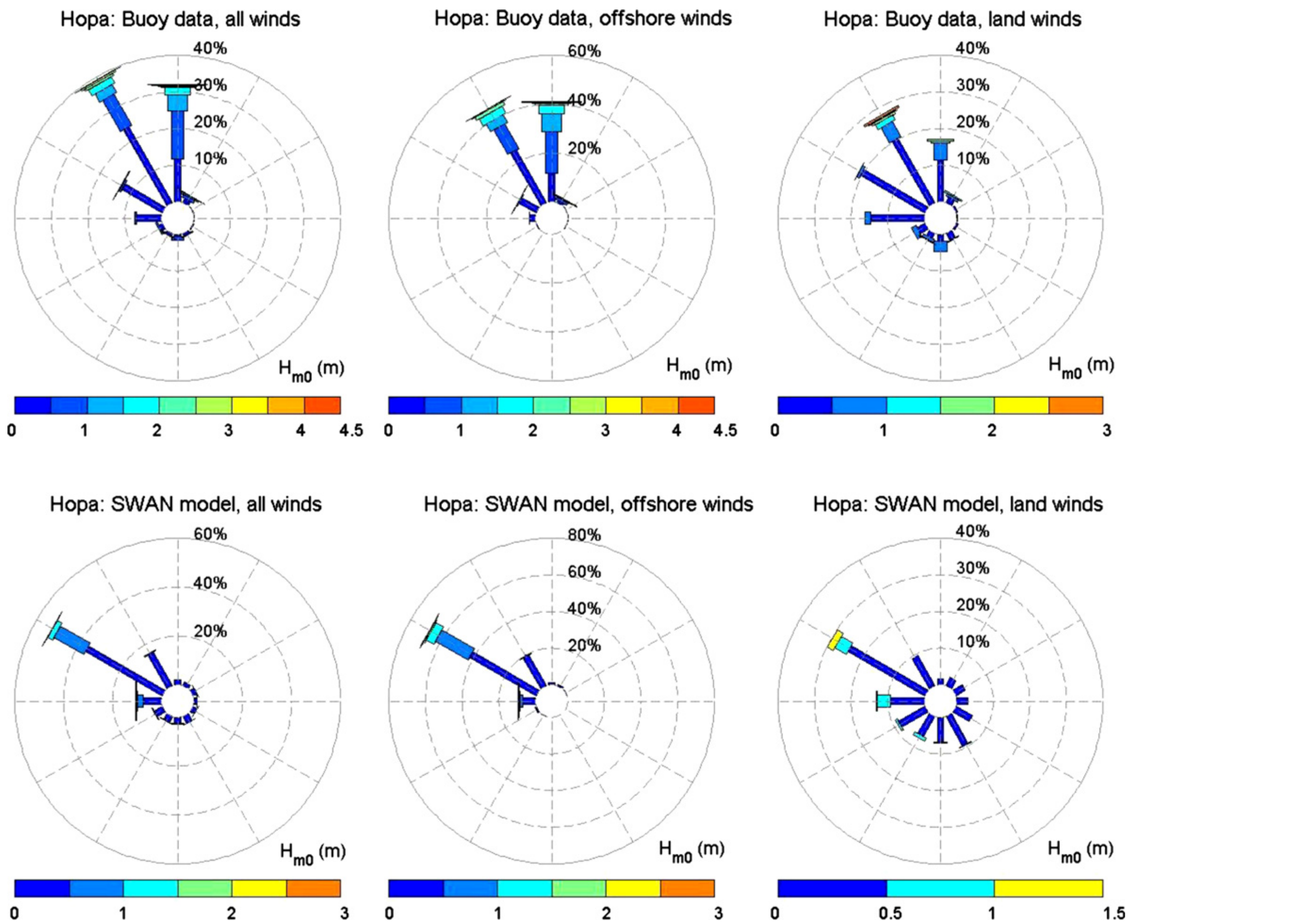

Fig. 18. Corresponding directional wave spectra for all winds, offshore winds, and land winds for both measured and simulated data at Hopa buoy station.

variation of the significant wave height over depth ratio (H_{m0}/d) for storm instant 25 Jan 1995, 00:00 h. It can be seen that the highest values are found along the eastern edges of the Sea of Azov. Finally, it is found a very small area along the western edge where triads and surf breaking play any role. For the rest of the Black Sea it is too deep to have shallow water effects on wave evolution. Therefore, shallow water effects only appear in the shelf margins in the west and north, at least for this typical storm situation.

6. Summary and conclusions

The SWAN model was successfully implemented for the Black Sea with the purpose of constituting a database for various wave parameters. This database can then be used for comprehensive examinations of wave energy potential, long-term changes in wind-wave climate, and performing extreme value statistics to come up with design parameters. To validate the SWAN model, measured data were obtained from three buoys, and also, SWAN model results were compared with a parametric model results and METU3 hindcasts showing that the present SWAN model can be considered as an improvement over the METU3 model. Finally, the SWAN model results show a similar trend with the measurements in the temporal variations of significant wave height and average wave period (T_{m02}), but it still has lower estimates for the maximum values of both parameters. This lower estimation is probably due to low wind speeds, which is probably affected by orographic effects in the ECMWF wind fields, and due to the relatively course resolution in time and space of the ERA-Interim wind fields for the Black Sea.

The SWAN model obtained more accurate estimates of wave parameters in Gelendzhik station compared to other two stations and in Hopa station compared to Sinop station. This is probably due to the more exposed location of the Gelendzhik buoy. The model slightly overestimates low wave heights and underestimates high values of the significant wave height. The correlation coefficients between the observed and simulated significant wave height are higher than those of average wave periods (T_{m02}) and directions at both Hopa and Sinop buoy stations.

The SWAN model outperforms the JONSWAP predictions for two wave parameters. Besides, the model has also better estimates for the peak and trough values in the time series of significant wave height compared to METU3 hindcasts. The reasons may be both the increase of the quality of the input data and recent advances in the modelling systems used due to increasing knowledge of wave processes and wind-wave generation mechanism.

The present analysis of wave model performance of is rather limited as only time series of the significant wave height H_{m0}, the spectral period T_{m02} and the mean wave direction DIR were available from the buoy analysis for comparing with the SWAN model results. In our opinion, only using T_{m02} as a measure for a wave period, does not provide a proper picture of model performance as this parameter is rather sensitive to errors in the wind forcing and as it does not really represent the energy containing part of the spectrum. For a more complete assessment of model performance using the spectral periods T_{m01} and $T_{m\text{-}1,0}$, as well as

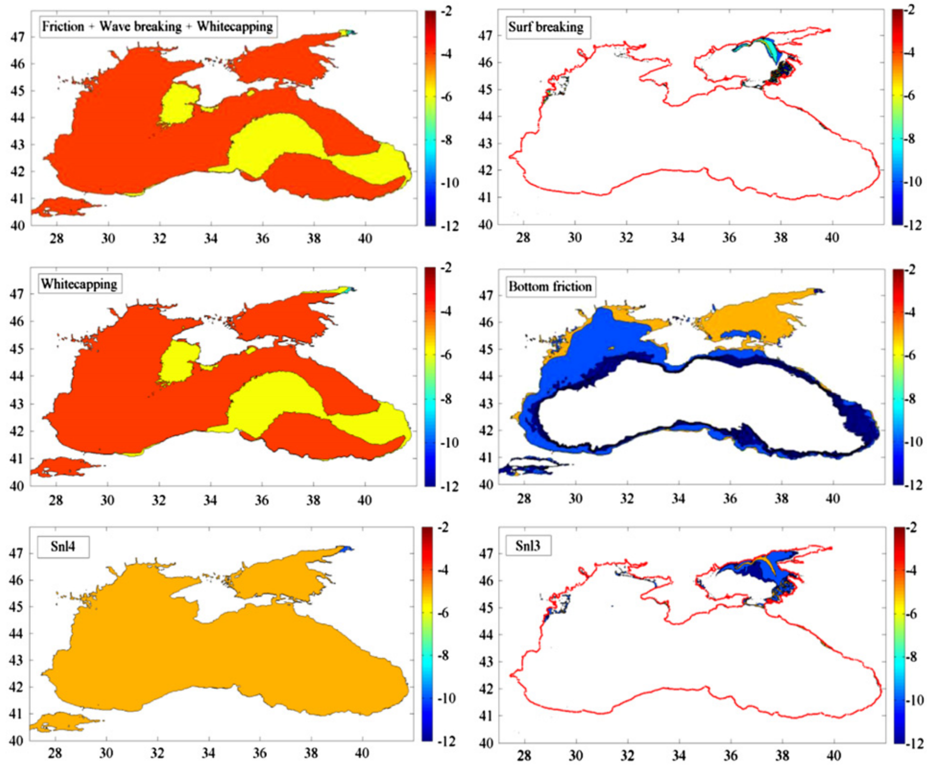

Fig. 19. Spatial variations of the logs of the strengths of the normalized source term magnitudes for non-linear four-wave interactions, whitecapping, and energy dissipation due to bottom friction, wave breaking, and whitecapping (left-hand panels), and for non-linear three-wave interactions, bottom friction, and surf breaking (right-hand panels). Storm instant of 25 January 1995, 00:00 h.

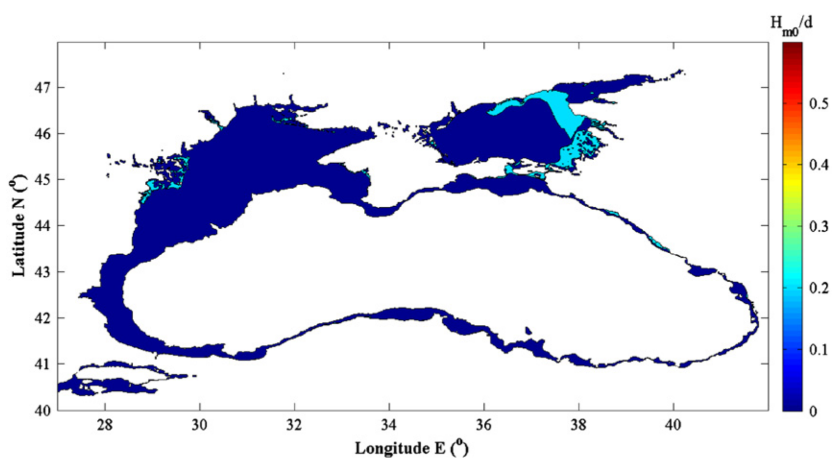

Fig. 20. Variation of wave height over depth ratio H_{m0}/d for storm instant 25 Jan1995, 00:00 h.

the directional spreading DSPR is advised as they provide valuable information to judge model performance.

The Black Sea is rather deep as can be seen from the shallow water aspects analysis. Only at the edges of the Black Sea, shallow water processes become significant, causing enhanced gradients in wave conditions. Therefore, we expect that for nearshore predictions, the present spatial resolution is possibly too crude. Also, for land winds the spatial resolution may be to coarse to accurately predict wave growth at short fetches. A simple solution to this problem is to apply the nesting facilities of the SWAN model, or to apply unstructured grids with varying spatial resolution. In addition, validation and calibration of wind fields against satellite data is recommended as well as applying wind fields with a finer spatial and temporal resolution to further improve the quality of our Black Sea wave model.

Acknowledgements

The authors would like to thank the ECMWF for providing the wind forcing data, the TSMS (Turkish State Meteorological Service) for its helps in recruiting the necessary permissions for obtaining data from the ECMWF, and NOAA (Geophysical Data Center) for the providing the bathymetry data of the Black Sea. The authors would like to acknowledge Prof. Dr. Erdal Özhan of the Middle East Technical University, Ankara, Turkey, who was the Director of the NATO TU-WAVES, for providing the buoy data, and the NATO Science for Stability Program for supporting the NATO TU-WAVES project. This study is a product of the PhD thesis of Adem Akpınar.

References

Abdalla, S., Özhan, E., 1994. METU models for wind-wave prediction. METU-KLARE Special Report. Middle East Technical University, Ankara, Turkey.

Abdalla, S., Özhan, E., Seziş-Papila, S., Gülçağ, O., 1995. An advanced third generation wind wave model for engineering use: application to the Black Sea and the Eastern Mediterranean. In: The Second International Conference on the Mediterranean Coastal Environment (MEDCOAST'95), October, Tarragona, Spain, Proceedings, pp. 1871–1884.

Akpınar, A., 2012. Wave modeling and wave energy potential determination in the Black Sea, PhD Thesis last progressive report, Karadeniz Technical University, The Graduate School of Natural and Applied Sciences, Trabzon, Turkey.

Akpınar, A., Kömürcü, M.İ., Özger, M., Kankal, M., 2011. The application of the SWAN model for wave simulation in the Black Sea. In: Proceedings of 7th Coastal Engineering Conference, November 21–23, Trabzon, Turkey, pp. 269–280.

Ardhuin, F., Herbers, T.H.C., Watts, K.P., van Vledder, G.Ph., Jensen, R., Graber, H., 2007. Swell and slanting fetch effects on wind wave growth. Journal of Physical Oceanography 37, 908–931.

Ardhuin, F., Rogers, E., Babanin, A.V., Filipot, J-F., Magne, R., Roland, A., Van der Westhuysen, A., Queffeulou, P., Lefevre, J-M., Aouf, L., Collard, F., 2010. Semiempirical dissipation source functions for ocean waves. Part I: Definition, calibration, and validation. Journal of Physical Oceanography 40, 1917–1941.

Battjes, J.A., 1994. Shallow water wave modeling. In: Proceedings of International Symposium: Waves—Physical and Numerical Modeling, University of British Columbia, Vancouver, pp. 1–23.

Battjes, J.A., Janssen, J.P.F.M., 1978. Energy loss and set-up due to breaking of random waves. In: Proceedings of 16th International Conference on Coastal Engineering, ASCE, pp. 569–587.

Battjes, J.A., Van Vledder, G.Ph., 1984. Verification of Kimura's theory for wave group statistics. In: Proceedings of 19th International Conference on Coastal Engineering, ASCE, Houston, pp. 642–648.

Bidlot, J.R., Holmes, D.J., Wittmann, P.A., Lalbeharry, R., Chen, H.S., 2002. Intercomparison of the performance of operational ocean wave forecasting systems with buoy data. Weather and Forecasting (American Meteorological Society 17, 287–310.

Booij, N., Holthuijsen, L.H., Ris, R.C., 1999. A third-generation wave model for coastal regions. 1 Model description and validation. Journal of Geophysical Research 104 (C4), 7649–7666.

Bretschneider, C.L., 1970. Wave forecasting relations for wave generation. Look Lab, Hawaii 1 (3).

Caires, S., Sterl, A., Bidlot, J.R., Graham, N., Swail, V., 2004. Intercomparison of different wind-wave reanalysis. Journal of Climate (American Meteorological Society 17 (10), 1893–1913.

Cavaleri, L., 2009. Wave modeling—missing the peaks. Journal of Physical Oceanography 39, 2757–2778.

Cavaleri, L., Malanotte-Rizzoli, P., 1981. Wind wave prediction in shallow water: theory and applications. Journal of Geophysical Research 86 (C11), 10961–10973.

Cavaleri, L., Alves, J.-H.G.M., Ardhuin, F., Babanin, A., Banner, M., Belibassakis, K., Benoit, M., Donelan, M., Groeneweg, J., Herbers, T.H.C., Hwang, P., Janssen, P.A.E.M., Janssen, T., Lavrenov, I.V., Magne, R., Monbaliu, J., Onorato, M., Polnikov, V., Resio, D., Rogers, W.E., Sheremet, A., McKee Smith, J., Tolman, H.L., van Vledder, G., Wolf, J., Young., I., 2007. Wave modeling—the state of the art. Progress in Oceanography 75 (4), 603–674.

Cherneva, Z., Andreeva, N., Pilar, P., Valchev, N., Petrova, P., Soares, C.G., 2008. Validation of the WAMC4 wave model for the Black Sea. Coastal Engineering 55, 881–893.

Collins, J.I., 1972. Prediction of shallow water spectra. Journal of Geophysical Research 77 (15), 2693–2707.

Dee, D.P., Uppala, S.M., Simmons, A.J., Berrisford, P., Pol, P., Kobayashi, S., Andrae, U., Balmaseda, M.A., Balsamo, G., Bauer, P., Bechtold, P., Beljaars, A.C.M., van de Berg, L., Bidlot, J., Bormann, N., Delsol, C., Dragani, R., Fuentes, M., Geer, A.J., Haimberger, L., Healy, S.B., Hersbach, H., Holm, E.V., Isaksen, L., Kallberg, P., Köhler, M., Matricardi, M., McNally, A.P., Monge-Sanz, B.M., Morcrette, J.-J., Park, B.-K., Peubey, C., de Rosnay, P., Tavolato, C., Thepaut, J.-N., Vitart, F., 2011. The ERA-Interim reanalysis: configuration and performance of the data assimilation system. Quarterly Journal of the Royal Meteorological Society 137, 553–597.

Donelan, M.A., 1980. Similarity theory applied to the forecasting of wave heights, periods and directions. In: Proceedings of Canadian Coastal Conference, National Research Council of Canada, pp. 47–61.

Eldeberky, Y., 1996. Nonlinear transformation of wave spectra in the nearshore zone. Ph.D. Thesis. The Delft University of Technology, Department of Civil Engineering, The Netherlands.

Eldeberky, Y., Battjes, J.A., 1996. Spectral modeling of wave breaking: application to Boussinesq equations. Journal of Geophysical Research 101 (C1), 1253–1264.

Hasselmann, K., 1974. On the spectral dissipation of ocean waves due to white-capping. Boundary-Layer Meteorology 6 (1–2), 107–127.

Hasselmann, K., Barnett, T.P., Bouws, E., Carlson, H., Cartwright, D.E., Enke, K., Ewing, J.A., Gienapp, H., Hasselmann, D.E., Kruseman, P., Meerburg, A., Mller, P., Olbers, D.J., Richter, K., Sell, W., Walden, H., 1973. Measurements of wind-wave growth and swell decay during the Joint North Sea Wave Project (JONSWAP), Ergnzungsheftzur Deutschen Hydrographischen Zeitschrift Reihe. Deutsches Hydrographisches Institute, Hamburg, Germany 95pp.

Hasselmann, S., Hasselmann, K., Allender, J.H., Barnett, T.P., 1985. Computations and parameterizations of the linear energy transfer in a gravity wave spectrum, Part II: parameterizations of the nonlinear transfer for application in wave models. Journal of Physical Oceanography 15 (11), 1378–1391.

Holthuijsen, L.H., Booij, N., Ris, R.C., 1993. A spectral wave model for the coastal zone. In: Proceedings 2nd International Symposium on Ocean Wave Measurement and Analysis, New Orleans, Louisiana, July 25–28, New York, pp. 630–641.

Holthuijsen, L.H., Zijlema, M., van der Ham, P.J., 2008. Wave physics in a tidal inlet. In: Proceedings 31st International Conference on Coastal Engineering. Hamburg, Germany, pp. 437–448.

Isaaks, E.H., Srivastava, R.M., 1989. An Introduction to Applied Geostatistics. Oxford University Press, New York 561 pp.

Janssen, P.A.E.M., 1989. Wave induced stress and the drag of air flow over sea water. Journal of Physical Oceanography 19, 745–754.

Janssen, P.A.E.M., 1991. Quasi-linear theory of wind-wave generation applied to wave forecasting. Journal of Physical Oceanography 21, 1631–1642.

Journel, A.G., Huijbregts, C.J., 1978. Mining Geostatistics. Academic Press, London.

Kahma, K.K., Calkoen, C.J., 1992. Reconciling discrepancies in the observed growth rates of wind waves. Journal of Physical Oceanography 22, 1389–1405.

Kazeminezhad, M.H., Etemad-Shahidi, A., Mousavi, S.J., 2005. Application of fuzzy inference system in the prediction of wave parameters. Ocean Engineering 32 (14–15), 1709–1725.

Komen, G.J., Hasselmann, S., Hasselmann, K., 1984. On the existence of a fully developed windsea spectrum. Journal of Physical Oceanography 14, 1271–1285.

Krige, D.G., 1951. A statistical approach to some mine valuations and allied problems at the Witwatersrand. Master's Thesis, The University of Witwatersrand, South Africa.

Lin, W., Sanford, L.P., Suttles, S.E., 2002. Wave measurement and modeling in Cheasepeake Bay. Continental Shelf Research 22, 2673–2686.

Madsen, O.S., Poon, Y.K., Graber, H.C., 1988. Spectral wave attenuation by bottom friction: theory. In: Proceedings of 21st International Conference on Coastal Engineering, ASCE, pp. 492–504.

Matheron, G., 1963. Principles of geostatistics. Economic Geology 58, 1246–1266.

Miles, J.W., 1957. On the generation of surface waves by shear flows. Journal of Fluid Mechanics 3, 185–204.

Moeini, M.H., Etemad-Shahidi, A., 2007. Application of two numerical models for wave hindcasting in Lake Erie. Applied Ocean Research 29, 137–145.

Moeini, M.H., Etemad-shahidi, A., 2009. Wave parameter hindcasting in a lake using the SWAN model. Transaction A: Civil Engineering 16 (2), 156–164.

Moeini, M.H., Etemad-Shahidi, A., Chegini, V., 2010. Wave modeling and extreme value analysis off the Northern Coast of the Persian Gulf. Applied Ocean Research 32, 209–218.

Özger, M., 2007. Wave energy hindcast and stochastic modelling. Ph.D. Thesis, İstanbul Technical University, The Graduate School of Natural and Applied Sciences, İstanbul, Turkey.

Özger, M., Şen, Z., 2007. Triple diagram method for the prediction of wave height and period. Technical Notes. Ocean Engineering 34, 1060–1068.

Özhan, E., Abdalla, S., 1998. Wind-wave climate of the Black Sea and the Turkish coast (NATO TU-WAVES project). In: Proceedings of 5th International Workshop on Wave Hindcasting and Forecasting, January 27–30, Melbourne, Florida, USA, pp. 71–82.

Özhan, E., Abdalla, S., Seziş-Papila, S., Turhan M., 1995. Measurements and modelling of wind-waves along the Turkish Mediterranean Coasts and the Black Sea. In: Proceedings of the Second International Conference on the Mediterranean Coastal Environment, MEDCOAST'95, October 24–27, Tarragona, Spain.

Özhan, E., Abdalla, S., Yilmaz, N., 2003. Wind and wave climate of the Black Sea. In: Proceedings of 2nd International Conference on Oceanography of the Eastern Mediterranean and the Black Sea, Ankara, Turkey, pp. 189–195.

Phillips, O.M., 1957. On the generation of waves by turbulent wind. Journal of Fluid Mechanics 2, 417–445.

Pierson, W.J., Moskowitz, L., 1964. A proposed spectral form for fully developed seas based on the similarity theory of S.A. Kitaigorodskii. Journal of Geophysical Research 69, 5181–5191.

Ponce de Leon, S., Orfila, A., Gomez-Pujol, L., Vizoso, G., Tintore, J., 2012. Assessment of wind models around the Balearic Islands for operational wave forecast. Applied Ocean Research 34, 1–9.

Reeve, D., Chadwick, A., Fleming, C., 2004. Coastal Engineering: Processes, Theory, and Design Practice. Spon Press, Taylor and Francis Group, London and New York.

Ris, R.C., Holthuijsen, L.H., Booij, N., 1994. A spectral model for waves in the near shore zone. In: Proceedings of 24th International Conference on Coastal Engineering, Kobe, October 1994, Japan, pp. 68–78.

Ris, R.C., Holthuijsen, L.H., Booij, N., 1999. A third-generation wave model for coastal regions: 2 Verification. Journal of Geophysical Research 104 (C4), 7667–7681.

Rzheplinkskij, G., 1969. Wind and wave atlas of the Black Sea. Gidrometeoizdat, Leningrad 111 in Russian.

Rogers, W.E., Hwang, P.A., Wang, D.W., 2003. Investigation of wave growth and decay in the SWAN model: three regional-scale applications. Journal of Physical Oceanography 33, 366–389.
Rusu, E., 2009. Wave energy assessments in the Black Sea. Journal of Marine Science and Technology 14 (3), 359–372.
Rusu, L., 2010a. Application of numerical models to evaluate oil spills propagation in the coastal environment of the Black Sea. Journal of Environmental Engineering and Landscape Management 18 (4), 288–295.
Rusu, E., 2010b. Modelling of wave–current interactions at the mounths of the Danube. Journal of Marine Science and Technology 15 (2), 143–159.
Rusu, L., Ivan, A., 2010. Modelling wind waves in the Romanian coastal environment. Environmental Engineering and Management Journal 9 (4), 547–552, http://dx.doi.org/10.1007/s00773-009-0078-x.
Signell, R.P., Carniel, S., Cavaleri, L., Chiggiato, J., Doyle, J.D., Pullen, J., Sclavo, M., 2005. Assessment of wind quality for oceanographic modelling in semi-enclosed basins. Journal of Marine Systems 53, 217–233.
SWAN team, 2012. SWAN user manual. SWAN Cycle III version 40.85 Delft University of Technology. Technical Documentation, 94 pp.
Sorkina, A.I., 1974. Climatic Handbook of the Black Sea. M. Gidrometeoizdat 406 in Russian.
Terziev, F., 1991. Hydrometeorology and hydrochemistry of the USSR seas, Vol. 4—'The Black Sea', No 1—Hydro-meteorological Conditions. Gidrometeoizdat, S. Peterburg, 429 pp (in Russian).
Tolman, H.L., 1991. A third-generation model for wind waves on slowly varying, unsteady and inhomogeneous depths and currents. Journal of Physical Oceanography 21, 782–797.
Tolman, H.L., 1999. User manual and system documentation of WAVEWATCH III version 1.18, NOAA/NWS/NCEP/OMB technical note 166, 100 pp.
Tolman, H.L., Banner, M.L., Kaihatu, J.M., 2011. The NOPP operational wave model improvement project. In: Proceedings of the 12th International Workshop on Wave Hindcasting and Forecasting, Kohala Coast, Hawaii, HI, USA.
U.S. Army, 1984. Shore Protection Manual, U.S. Army Engineer Waterways Experiment Station, U.S. Government Printing Office, fourth ed. –No. 20402,Washington, DC, USA, 652 pp.
U.S. Army, 2003. Coastal engineering manual, chapter II-2, meteorology and wave climate, U.S. Army Engineer Waterways Experiment Station, U.S. Government Printing Office, No. EM 1110-2-1100, Washington DC, USA, 77 pp.
Valchev, N., 2008. Hindcasting and assessment of the Western Black Sea wind and wave climate. In: 2nd Biannual and Black Sea Scene EC Project Joint Conference, 6–9 October, Sofia, Bulgaria, pp. 43–51.
Van der Westhuysen, A.J., 2002. The application of the numerical wind-wave model SWAN to a selected field case on the South African Coast. M.Sc. Thesis, The University of Stellenbosch, South Africa, 198 pp.
WAMDI Group, 1988. The WAM model—a third generation ocean wave prediction model. Journal of Physical Oceanography 18, 1775–1810.
Wilson, B.W., 1965. Numerical prediction of ocean waves in the North Atlantic for December, 1959. Ocean Dynamics 18 (3), 114–130.
Young, I.R., Van Vledder, G.Ph., 1993. A review of the central role of nonlinear interactions in wind-wave evolution. Philosophical Transactions of the Royal Society A: Mathematical, Physical & Engineering Sciences 342, 505–524.
Yüksel, Y., Çevik, E.Ö., 2009. Coastal engineering, Marine Engineering Series—No. 1. Beta Publishing Co., Istanbul, Turkey 732 pp.
Zijlema, M., Van der Westhuysen, A.J., 2005. On convergence behaviour and numerical accuracy in stationary SWAN simulations of nearshore wind wave spectra. Coastal Engineering 52 (3), 237–256.